ACS OMEGA

http://pubs.acs.org/journal/acsodf

Article

Addressing the Exigent Role of a Coumarin Fluorophore toward Finding the Suitable Microenvironment of Biomimicking and Biomolecular Systems: Steering to Project the Drug Designing and Drug Delivery Study

Sandip Paul, Pritam Roy, Sourav Das, Soumen Ghosh, Pinki Saha Sardar,* and Anjoy Majhi*

Cite This: *ACS Omega* 2021, 6, 11878−11896

Read Online

ACCESS | Metrics & More | Article Recommendations | Supporting Information

ABSTRACT: The photophysics of 4-azidocoumarin (4-AC), a novel fluorescent coumarin derivative, is well established by the investigation of the alteration of the microheterogeneous environment comprising two types of systems: supramolecular systems, cyclodextrins (CDs), and biomolecular systems, serum albumins (SAs). The enhanced emission of the ligand with the organized assemblies like α-CD, β-CD, and γ-CD by steady-state and time-resolved fluorescence and fluorescence anisotropy at 298 K is compared with those of bovine serum albumin (BSA) and human serum albumin (HSA). The remarkable enhancement of the emission of ligand 4-AC along with the blue shift of the emission for both the systems are visualized as the incorporation of 4-AC into the hydrophobic core of the CDs and proteins mainly due to reduction of nonradiative decay process in the hydrophobic interior of CDs and SAs. The binding constants at 298 K and the single binding site are estimated using enhanced emission and anisotropy of the bound ligand in both the systems. The marked enhancement of the fluorescence anisotropy indicates that the ligand molecule experiences a motionally constrained environment within the CDs and SAs. Rotational correlation time (θ_c) of the bound ligand 4-AC is calculated in both the categories of the confined environment using time-resolved anisotropy at 298 K. Molecular docking studies for both the variety of complexes of the ligand throw light to assess the location of the ligand and the microenvironment around the ligand in the ligand−CD and ligand−protein complexes. Solvent variation study of the probe 4-AC molecule in different polar protic and aprotic solvents clearly demonstrates the polarity and hydrogen-bonding ability of the solvents, which supports the alteration of the microenvironments around 4-AC due to binding with the biomimicking as well as biomolecular systems. Dynamic light scattering is employed to determine the hydrodynamic diameter of free BSA/HSA and complexes of BSA/HSA with the ligand 4-AC.

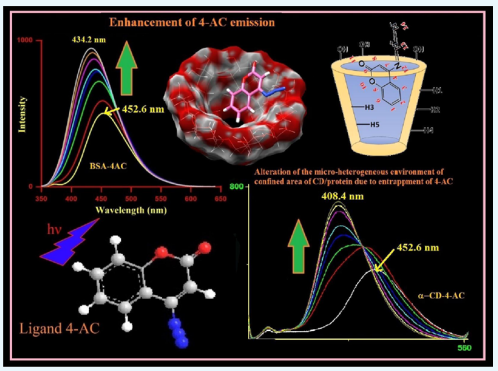

INTRODUCTION

The microenvironment responsive ligands or drugs have been an emergent application in the recent times for investigations on drug designing or drug delivery research. Perturbation or alteration of the microenvironment surrounding a ligand/drug molecule is a prime concern of the current medical science and life science projects.[1−9] The nature of the microenvironment surrounding a ligand or drug or any other molecule has been explored by a variety of spectroscopic techniques, among which fluorescence spectroscopy seems to be the most widely used technique.[2,10−12] Fluorescent probes are powerful tools for biosensing and bioimaging because of their high sensitivity, specificity, high fluorescence intensity, excellent solubility, biocompatibility, and simple preparation.[13] Hence, development of fluorescent probes, specifically for biological settings and clinical settings, has attracted intense interest.[13−16] Till date, different kinds of fluorescent probes are commercially available and can be used in biological investigations.[13] Coumarin molecules, as a family of molecules, exhibit a wide range of fluorescence emission properties; hence, they are used as a fluorescent probe, and they also have a wide range of biological importance.[17−26] For example, azidocoumarins are known to be used in biomolecular photoaffinity labelling.[27] It may also be noted that photostability is an important criteria for a molecule to become a good fluorescent probe.[28] The use of fluorescent probes in some biomolecular systems and biomimicking systems, in many times, helps to amend some structural change of these systems, advocating the challenging roles of those probes toward the environments.[3−6,9,29−32]

Received: January 10, 2021
Accepted: April 9, 2021
Published: April 22, 2021

The fluorescent probe containing polar groups have enormous features in their solvatochromic studies as fluorescence emission maxima and quantum yield are very much dependent on the nature of the solvents.[33] The polarity/polarizability, refractive index, and dielectric constant of the solvent molecules or the intermolecular hydrogen bonding between the fluorophore and the solvent[33−35] modulates the photophysics of the excited state of the fluorophore and also the microenvironment of the fluorophore.[33−35] Hence, thorough studies on several coumarin dyes report that the coumarin molecules are very much dependent on solvent polarity which govern the fluorescence quantum yield and also the local environment of the molecule where they are situated.[36,37] Hence, these solvent dynamic studies of coumarin dye molecules might play an imperative role in use as a fluorescent biomarker.[38−41]

The photophysical processes of the ligands/drugs exploiting the biomimicking systems have achieved enormous attention for the biological processes occurring in the molecular level. Several organized assemblies or supramolecular hosts like cyclodextrins (CDs), micelles, reverse micelles, lipids, microemulsions, vesicles, membranes, crown ethers, cryptands, calixarenes, and cucurbiturils are promising encapsulating compounds which have versatile use in mimicking the biomolecular systems to address their microenvironment in the drug-binding study and in specific delivery of the drug.[9,32,42−45] One of the most important and promising host among these is the CD molecules. CD molecules are widely used as a molecular container in the pharmaceutical industry, biochemistry, material chemistry, catalysis, and electronics with proficient entrapment of the ligand/drug molecule having comparable sizes forming host−guest supramolecular complexes, which are the mimicking model of the enzyme/protein−ligand/drug complexes.[29,30,32,42,43,46−50] CD molecules have the ability to alter the physical, chemical, and biological properties of guest molecules through the formation of inclusion complexes by capturing suitable hydrophobic guests into the hydrophobic cavity in aqueous media without forming a covalent bond.[32,46,47,49,51] Generally, CDs are α, β, and γ types containing 6, 7, and 8 glucopyranose units, respectively. The CD molecules have an internal cavity accessible to the guest molecules of proper dimension through an opening of 4.5−5.3, 6.0−7.0, and 7.5−8.5 Å for α-CD, β-CD, and γ-CD, respectively; the depths of all remaining are more or less the same (7.9 Å).[32,46,47,49,51] The hydrophobic cavity with a constrained environment directs one probe or ligand molecule to form encapsulated complexes with a proper geometry inside the microenvironment of the CD cavity.[32,46,47,49,51] Such investigations in present day research exploiting photophysical aspects have gained interest to sense the various photoprocesses with exact mechanism[32,46,47,49,51] like excited--state proton transfer,[32] intramolecular charge transfer, and so on.[34,35]

The interactions of a fluorescent probe with the biomimicking molecules are taken into deliberation to demonstrate the microenvironment of the biomolecules.[4−6] Human serum albumin (HSA) is a globular protein consisting of 585 amino acids, whereas bovine serum albumin (BSA) consists of 582 amino acids and is cross-linked by 17 disulfide bonds, and it shows 76% similarity to BSA.[23] The beauty of these proteins in physiological function is to bind and transport several molecules like fatty acids, nutrients, steroids, and other important drugs.[19,52,53] Therefore, researchers are studying their interaction and binding properties with other molecules and ligands, and they have been extensively explored.[5,54−59] Recently, interactions of several molecules, viz., anti-cancer drug crizotinib and angiotensin-converting enzyme inhibitor ramipril and lisinopril, with BSA have been reported.[60−62]

The aim of the work presented here is to explore the prospective expediency of the optical properties of the ligand 4-azidocoumarin (4-AC) (Scheme 1) and its interaction with

Scheme 1. Molecular Structure of 4-AC or 4-Azido-2*H*-chromen-2-one (Considering the Atom Numbering for Molecular Docking Studies (Not the Regular IUPAC Numbering[6])[a]

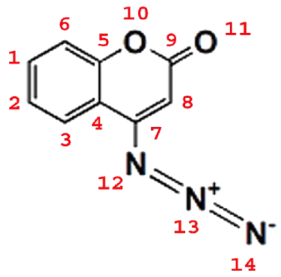

[a]Adapted with permission from ref 6. Copyright The Royal Society of Chemistry and the Centre National de la Recherche Scientifique 2017.

the relevant biomolecules or biomimicking molecules to demonstrate the microenvironment inside the biomolecules or biomimicking molecules. The alteration of the microenvironment inside the CD cavity or protein nanocore after inclusion of the fluorophore was investigated by steady-state and time-resolved emission studies at 298 K by monitoring the enhancement of 4-AC emission due to interaction with all CD molecules and serum albumin (SA) proteins in an aqueous buffer medium of pH 7, which impelled us to understand the nature of binding and location of binding of the ligand in the CD (s) and protein (s). The modulation of the photophysics of 4-AC in the presence of CD and proteins has been utilized to determine the binding constants of the complexes and the binding site (s) of the CD and proteins probing the enhanced emission of the bound ligand at 298 K. The variation of steady-state anisotropy data of the bound ligand in CDs and SAs has been utilized to find out the gradual increase of rigidity of environment of the ligand in the complexes. The time-resolved anisotropy of the complexes of the ligand in the presence of CD and protein by monitoring the ligand emission has been measured to determine the rotational constant values (θ_c) of the ligand 4-AC, which helps us to substantiate the interaction of the ligand with the CD and protein molecules and the nature of perturbation of the ligand environment in all CD molecules and both the SAs, as revealed in the molecular docking studies. Also, the nature of environment could be visualized by understanding the effect of polarity of different polar protic and aprotic solvents by the room temperature steady-state and time-resolved emission studies. Also, the change in hydrodynamic diameter upon ligand binding calculated from the dynamic light scattering (DLS) data concludes that the ligand induced perturbation of the microenvironment of SAs. Thus, the modulation of the photophysics of 4-AC in the presence of different microheterogeneous environments might be supportive to show the

https://doi.org/10.1021/acsomega.0c06152
ACS Omega 2021, 6, 11878−11896

Table 1. Photophysical Data of 4-AC in Solvents of Different Polarities at 298 K

solvents	λ_{max} for emission (nm)	$\Delta\upsilon$ (cm^{-1})	π^*[a]	α[b]	β[c]	$E_T(30)$[d] (kcal/mol)	dielectric constant (ε)	quantum yield (φ)	lifetime (ns) $\tau_1(\alpha_1)$ (ns)	lifetime (ns) $\tau_2(\alpha_2)$ (ns)	lifetime (ns) τ_{av}[e] (ns)	lifetime (ns) χ^2	rate of the radiative transition ($k_r \times 10^{-7}$) (s^{-1})	rate of the nonradiative transition ($k_{nr} \times 10^{-8}$) (s^{-1})
water	453.6	9010	1.09	1.17	0.18	63.1	78.36	0.056	4.94 (3.34%)	0.85 (96.66%)	0.99	0.96	5.66	9.54
EG	452.0	9126	0.88	0.90	0.52	56.3	37.7	0.033	4.95 (7.77%)	1.98 (92.23%)	2.21	1.21	1.49	4.38
MeOH	451.0	8787	0.60	0.93	0.62	55.5	32.6	0.035	4.94 (11.51%)	1.37 (89.49%)	1.79	0.91	1.96	5.39
EtOH	448.0	8734	0.54	0.83	0.77	51.9	22.4	0.021	4.02 (14.77%)	2.33 (85.23%)	2.58	1.22	0.81	3.79
isopropanol	450.0	9028	0.48	0.76	0.95	48.4	19.92	0.014	4.85 (31.76%)	1.90 (68.24%)	2.84	1.01	0.49	3.47
ACN	406.6	6558	0.73	0.00	0.69	46.0	37.5	0.026	4.43 (48.65%)	1.08 (51.35%)	2.71	1.21	0.96	3.59
DMSO	400.4	6081	0.98	0.00	0.76	45.0	46.6	0.236	5.52 (50.68%)	1.65 (49.32%)	3.61	1.26	6.54	2.11
benzonitrile	407.7	6722	0.90	0.00	0.41	41.5	25.9	0.012	5.69 (6.67%)	1.39 (93.33%)	1.68	1.22	0.71	5.88
DOX	403.8	6485	0.55	0.00	0.37	36.0	2.21	0.019	5.66 (47.84%)	1.77 (52.16%)	3.63	1.14	0.52	2.70

[a] π^* is the polarity or polarizability effects of the solvent. [b] α is the hydrogen bond donor acidity of the solvent. [c] β is the hydrogen bond acceptor basicity of the solvent. [d] $E_T(30)$ is the Dimroth–Reichardt empirical polarity parameter of the solvent. [e] Error in the measurements is ±0.1 ns.

https://doi.org/10.1021/acsomega.0c06152
ACS Omega 2021, 6, 11878−11896

efficacy of a ligand to open up new avenues toward targeted drug delivery projects.

RESULTS AND DISCUSSION

Steady-State and Time-Resolved Fluorescence Studies of 4-AC in Different Pure Solvents. *Understanding the Nature of Microenvironment around the Fluorophore.* Investigations of the microenvironment surrounding the fluorophore 4-AC using steady-state and time-resolved fluorescence spectroscopy of 4-AC in different polar protic and polar aprotic pure solvents were carried out. The absorption spectra in all cases show two absorption bands. One is the intense ($\pi-\pi^*$) band in the region 280−300 nm and the other is a relatively weak (n−π^*) in the region 310−350 nm. The absorption bands of 4-AC remain almost invariant in the presence of different solvents (figure not shown). The absorption band maxima of 4-AC in the presence of pure solvents are listed in Table 1. The single emission band was recorded monitoring the respective λ_{max} of the absorption band of 4-AC in various solvents, as shown in Figure 1. The

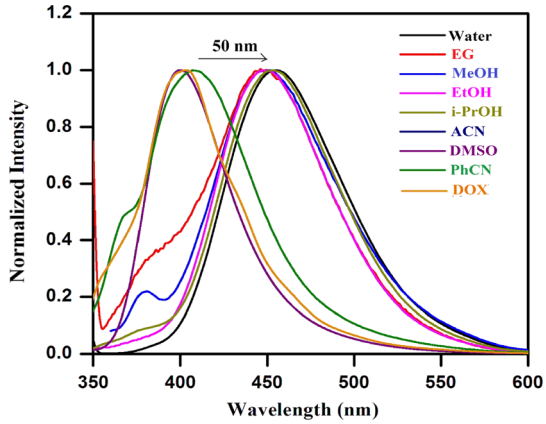

Figure 1. Fluorescence spectra of 4-AC at 298 K in different pure solvents. λ_{exc} = 330 nm; excitation and emission band pass = 10 and 5 nm, respectively.

positions of the emission band in different solvents are provided in Table 1. The emission maxima of 4-AC in different solvents are red-shifted with increasing polarity of the solvent. The red shift is ∼50 nm, which supports the polar nature of the emissive state, and the variations of the emission maxima of 4-AC in different solvents (Table 1) are in accordance with its empirical polarity parameters $E_T(30)$ by Reichardt.[63,64]

The emission of 4-AC molecule is governed by the polarity/polarizability π^*, hydrogen bond-donating ability α, and hydrogen bond-accepting ability β of different solvents,[63,64] and for this, Kamlet−Taft multiparameter approach[65] is used. These parameters for different solvents and the Stokes shift of emission of 4-AC in different solvents are provided in Table 1. A linear regression analysis has been employed considering all these parameters and the Stoke shift (Δ) in solvents of different polarities and gives the relation[65] (Figure S1)

$$\Delta = 8415.68 - 205.13\pi^* + 854.12\alpha - 1124.54\beta \quad (1)$$

Using all solvent parameters simultaneously, a well and good relationship between the Kamlet−Taft solvent parameters[65] and the Stokes shift emission of the 4-AC molecule is observed (Figure S1) [slight deviation is observed for isopropanol and dioxane (DOX)].This clearly put a signature of the dependence of the polarity, the hydrogen-bond donating ability, as well as the hydrogen bond-accepting ability of the solvents on the emission of 4-AC.

The plot of transition energy (E_T in kcal/mol) of the emission of 4-AC (10 μM) in different solvents against the solvent polarity index $E_T(30)$-scale (kcal/mol) by Reichardt[63,64] is presented in Figure 2A and found to be almost linear. The plot shows that the transition energy of the emission of 4-AC molecule decreases with the increase in the $E_T(30)$ value[63,64] of different solvents. This supports that the emissive state is stabilized with an increase in the solvent polarity index, and thus the emission shifts toward higher wavelength (Table 1). Also, the bathochromic shift of the emission maxima was also observed with increasing dielectric constant of the medium, especially when the polar protic solvent is used (Table 1). Figure 2B also represents the plot of transition energy of the emission of 4-AC in different polar protic solvents against the hydrogen bond-donating ability (α, Table 1) of the solvents. This reveals that the hydrogen bond-donating ability (α) of the polar protic solvents increases the stability of the emissive state, which again confirms the probe-solvent hydrogen-bonding interactions.

The quantum yield of emission of 4-AC in different polar protic and aprotic solvents is presented in Table 1. The plot of quantum yield against the hydrogen bond-donating ability (α) (Figure 2C) shows that the quantum yield decreases with decreasing α for the polar protic solvents, which determines the intermolecular hydrogen-bonding ability of 4-AC with the solvents, and also the polarity of the solvents operates in the determination of quantum yield of emission of 4-AC in polar protic solvents. For polar aprotic solvents (α = 0), the quantum yield increases as the polarity of the solvent (π^*-value) increases (some deviation observed for benzonitrile, Table 1). In dimethyl sulphoxide (DMSO), the quantum yield value is observed to be the highest (Table1).

Lifetime measurements monitoring the emission maxima of 4-AC molecules in different polar protic and aprotic solvents are recorded at 298 K using λ_{exc} = 290 nm. The lifetime values show biexponential decay in all solvents and are listed in Table 1. The plot of the average lifetime of the excited state and the $E_T(30)$ value of the different polar protic and aprotic solvents (Figure 2D) shows that the lifetime of the emissive state increases with a decrease in the $E_T(30)$ value from polar protic solvents to polar aprotic solvents. For water, the recovered lifetimes observed with a longer component 4.94 ns with a minor contribution (0.0334) and a shorter component 0.85 ns with a major contribution (0.9666) (Table 1) infer the presence of solvent-shielded 4-AC molecule and free 4-AC molecule, respectively. Both the components along with their contributions are changed with the change in polarity of the solvents (Table 1). The shorter lifetime component values (∼0.85 ns) are slightly increasing with the decrement of their percent contribution with change in the solvent polarity, which might be due to the intermolecular H-bonding interaction in different extent with the solvents having different polarity. This also confirms that the polarity and the hydrogen-bonding ability of 4-AC with other solvents are responsible for the enhancement of the lifetime from polar protic to polar aprotic solvents. The striking observation is that the lifetime components with the fractional contribution of 4-AC in DMSO (polar aprotic) and DOX (nonpolar) could be considered by the prevalence of specific solute−solvent interaction between the solvent and the probe molecule.

https://doi.org/10.1021/acsomega.0c06152
ACS Omega 2021, 6, 11878−11896

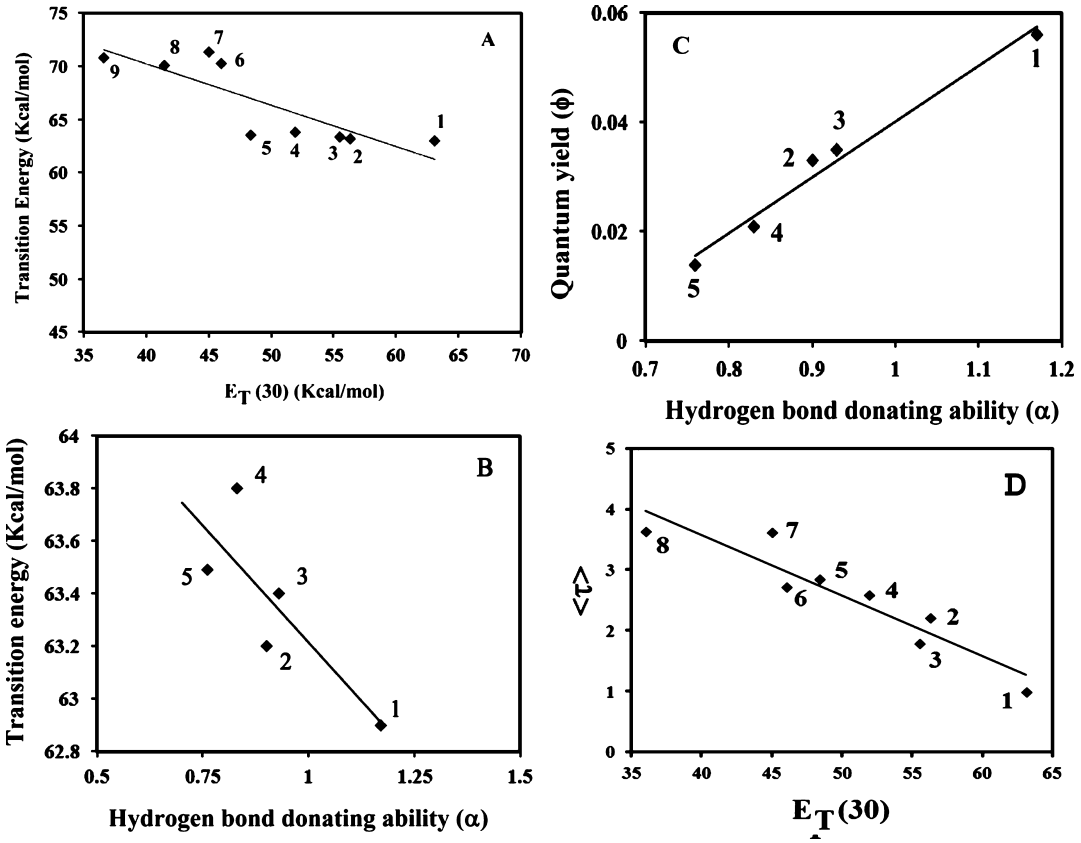

Figure 2. (A) Plot of transition energy (E_T in kcal/mol) of enhanced emission of 4-AC (10 μM) in different solvents against the solvent polarity index E_T(30)-scale (kcal/mol): (1) water, (2) EG, (3) methanol (MeOH), (4) ethanol (EtOH), isopropanol (*i*PrOH), (5) ACN, (6) DMSO, (7) benzonitrile (PhCN), and (8) DOX; λ_{exc} = 330 nm; excitation and emission band pass = 10 nm each. (B) Plot of transition energy (kcal/mol) of the emission of 4-AC in different solvents against the hydrogen bond-donating ability parameter alfa (α). (C) Plot of quantum yield against the hydrogen bond-donating ability parameter alfa (α). (D) Plot of average lifetime values of the solvents against the solvent polarity index E_T(30)-scale (kcal/mol).

The effect of the solvent polarity will also be judged by calculating the radiative[2] and nonradiative rate constants[2] in different solvents using eqs 2 and 3 and are provided in Table 1.

$$k_r = \varphi_f/\langle\tau_f\rangle \quad (2)$$

$$k_{nr} = \langle\tau_f\rangle^{-1} - k_r \quad (3)$$

It is observed that nonradiative decay rates are increased for polar protic solvents due to intermolecular hydrogen bonding of 4-AC with the polar solvent molecules. For DMSO, the nonradiative rate constant is found to be 2.11 × 10^8 s^{-1} compared to 9.54 × 10^8 s^{-1} in water (Table 1).

Photophysical Modulation of 4-AC in Biomimetic (Aqueous CD) Environments. *Steady-State Absorption and Fluorescence Studies of the Ligand 4-AC at 298 K.* The absorption spectra of 4-AC in the presence of different CD environments are provided in Figure 3. The absorption spectra are slightly changed on addition of CDs with no significant shift in λ_{max}, indicating the formation of host−guest complexes.

Figure 4 illustrates the modulation of the photophysics of 4-AC in the presence of confined environments of CD family and with respect to the intensity enhancement and shift of the emission maxima. The fluorescence spectra of the ligand 4-AC (10 μM) in aqueous buffer solution (pH 7) is characterized by a broad and unstructured band with a maxima at ∼452 nm (Figure 1) upon excitation at 290 nm. In aqueous buffer

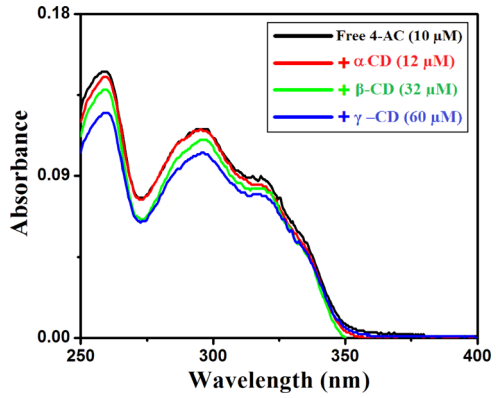

Figure 3. Absorption spectra of 4-AC (10 μM) in aqueous buffer and in the presence of α-CD, β-CD, and γ-CD solutions at 298 K.

solution, the fluorescence quantum yield (φ_D) of the ligand is very low (Table 2, Figure 1, and insets of Figure 4A−C). It increases with lowering of the polarity function (Figure 4A−C). The interactions of 4-AC with CD molecules are observed with a significant enhancement of the emission intensity along with considerable blue shifts of the emission maxima on gradual addition of α-CD, β-CD, and γ-CD to the aqueous buffer solution of pH 7 (Figure 4A−C). The shift of the emission wavelength for α-CD is ∼44 nm, for β-CD is ∼46 nm, and for γ-CD is ∼45 nm from the emission maxima of free

https://doi.org/10.1021/acsomega.0c06152
ACS Omega 2021, 6, 11878−11896

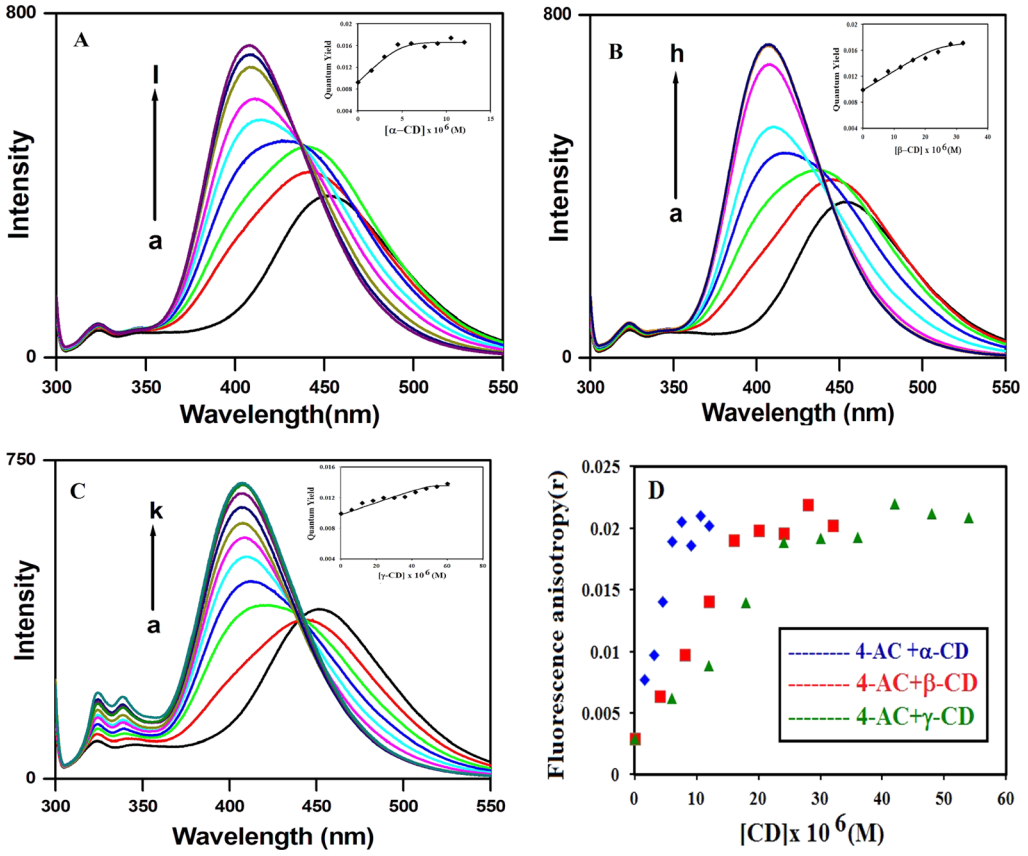

Figure 4. (A) Fluorescence spectra of 4-AC (10 μM) at 298 K with varying concentrations of α-CD; curves (a−i) represent 0, 1.5, 3.0, 4.5, 6.0, 7.5, 9.0, 10.5, and 12.0 μM α-CD, respectively; (B) fluorescence spectra of 4-AC (10 μM) at 298 K with varying concentrations of β-CD; curves (a−h) represent 0, 4.0, 8.0, 12.0, 16.0, 20.0, 24.0, and 32.0 μM β-CD, respectively; (C) fluorescence spectra of 4-AC (10 μM) at 298 K with varying concentrations of γ-CD; curves (a−k) represent 0, 6.0, 12.0, 18.0, 24.0, 30.0, 36.0, 42.0, 48.0, 54.0, and 60.0 μM γ-CD, respectively; λ_{exc} = 290 nm; excitation and emission band pass = 10 and 5 nm, respectively, in each case. Insets of (A−C): variation of fluorescence quantum yield (φ_F) of 4-AC (10 μM) in aqueous buffer monitoring the enhanced emission with increasing concentrations of α-CD, β-CD, and γ-CD, respectively. (D) Variation of fluorescence anisotropy (r) of 4-AC (10 μM) in aqueous buffer monitoring the enhanced emission with increasing concentrations of α-CD, β-CD, and γ-CD.

Table 2. Photophysical Parameters and Binding Parameters of 4-AC (10 μM) in the Presence of Different CD Systems at 298 K[a]

system	λ_{max}(nm)	quantum yield (φ_F) ($\times 10^2$)	<τ> (ns)	steady state anisotropy (r)	rotational correlation time (θ_c) (ns)	rate of the radiative transition ($k_r \times 10^{-7}$) (s^{-1})	rate of the nonradiative transition ($k_{nr} \times 10^{-8}$) (s^{-1})	binding constants[b] (K_b) (M^{-1}) (for 1:1 complex)	R^2	ΔG^0 (kJ mol^{-1})
buffer (pH 7)	452.6	0.991	0.99	0.00297		1.001	10.00			
α-CD (12 μM)	408.4	1.667	1.11	0.02108	2.098	1.502	8.86	6.38×10^5	0.9131	−33.12
β-CD (32 μM)	406.4	1.714	2.13	0.02192	1.941	0.805	4.69	3.17×10^5	0.9678	−31.38
γ-CD (60 μM)	407.2	1.382	2.64	0.02205	2.151	0.523	3.74	0.47×10^5	0.9512	−26.65

[a] λ_{exc} = 290 nm. [b] Error in the measurements is ±5%.

4-AC (~452 nm) (Figure 4, Table 2). This suggests that the inclusion of the ligand molecule is inside the hydrophobic core of the respective CD molecules, with the reduced polarity in the surroundings of the ligand molecule as compared to the bulk aqueous phase. The quantum yield (φ_D) of the enhanced emission of 4-AC (10 μM) in the presence of CDs is calculated (Table 2), and the variations of quantum yields of emission with the concentration of CD are provided in Figure 4. The enhancement of the fluorescence quantum yield values of 4-AC molecules in the presence of CD molecules is approximately 1.5 to 1.8 times as compared to that in aqueous buffer of pH 7. The lower value in the case of γ-CD indicates that the microenvironment surrounding the 4-AC molecule in γ-CD is more polar than those in the α-CD and β-CD molecules

https://doi.org/10.1021/acsomega.0c06152
ACS Omega 2021, 6, 11878−11896

(Table 2). The encapsulation of 4-AC molecule inside the CD cavity decreases the chances of intermolecular hydrogen bonding reaction of 4-AC with the solvent molecule (water/buffer), and therefore, deactivation of nonradiative decay channels, which operate through intermolecular H-bond through solvent molecules, results in the enhancement of the emission of the ligand molecule in the presence of the CD molecules.[32,46]

In our present work, the steady-state fluorescence studies of 4-AC molecule have also been carried out in the presence of varying concentrations of all CD molecules with excitation at 330 nm (i.e., near n−π^* transition) where the remarkable decrease in the fluorescence intensity of the 4-AC molecule was observed along with the appreciable blue shift of the emission maxima. The occurrence of this fluorescence quenching is probably due to the unavailability of nonbonding electrons present on the heteroatom of the 4-AC molecule. With the addition of increasing concentration of CDs, probably the nonbonding electrons present on the heteroatom of the 4-AC molecule are involved in the interaction with the polar group present on the outer part of CDs (−OH groups); hence the availability of nonbonding electrons becomes minimum to respond to the fluorescence of the 4-AC molecule, the possibility of n−π^* transition becomes less, and a reduction in the percentage of radiative decay is observed. A representative figure for the fluorescence quenching of 4-AC with the γ-CD-molecule is provided in Figure 5. This situation could be in use to assess the actual

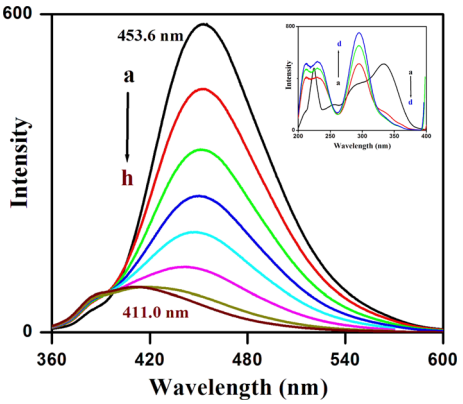

Figure 5. Fluorescence spectra of 4-AC (10 μM) at 298 K with varying concentrations of γ-CD; curves (a−h) represent 0, 6.0, 12.0, 18.0, 24.0, 30.0, 36.0, and 60.0 μM γ-CD, respectively; λ_{exc} = 290 nm; excitation and emission band pass = 10 and 5 nm, respectively, in each case. Inset: Fluorescence excitation spectra ($\lambda_{monitored}$ = λ_{max} of emission) of 4-AC in the presence of increasing concentration of γ-CD; curves (a−d) represent 0, 12.0, 30.0, and 60.0 μM γ-CD, respectively.

entrapped moiety inside the CD cavity as well as the part of the 4-AC molecule present in the bulk solvent. This occurrence might be suggesting the extent of efficiency of the host molecules to envelop the fluorophore from external perturbation, which increases the radiative processes. This observation can be rationalized from the molecular docking studies (see the next section).

The excitation spectra of the 4-AC molecule monitoring the corresponding enhanced emission of the 4-AC−CD complexes were measured. The representative excitation spectra for 4-AC−γ-CD complexes (inset of Figure 5) illustrate that the progressive increment of the 290 nm band with the disappearance of the 330 nm band clearly amplifies the role of π−π^* and n−π^* transitions in the emission processes of 4-AC molecule in the presence of varying concentrations of CD molecules.

Time-Resolved Fluorescence Studies of the Ligand 4-AC at 298 K. The modulation of the excited-state photophysics of a fluorescence probe in the presence of the microenvironment of some biomacromolecular (proteins/peptides/enzymes etc.)[2,4,9,56] or biomimetic (CD/micelle/lipid/vesicles etc.)[32,66] environment could be interpreted from the time-resolved fluorescence decay measurement. This technique helps to visualize the change in the lifetime values of the probe with the alteration of the microenvironment from the bulk aqueous region to the nanocore of the CD or protein molecules.

The lifetime of the probe 4-AC molecule in aqueous phosphate buffer of pH 7 was recovered and was best fitted as a biexponential function with an average lifetime value of 0.99 ns (100%) (Figure 6, Table 3), monitoring at 450 nm. The lifetime values including a fast component (∼0.85 ns) with a

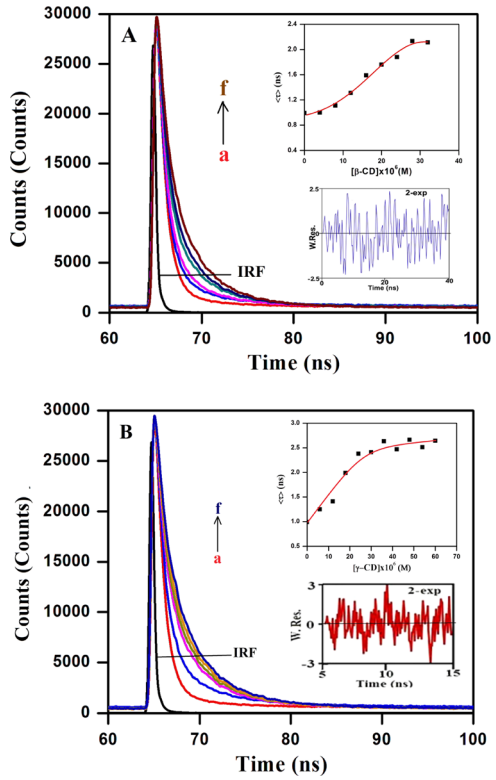

Figure 6. (A) Fluorescence decay of 4-AC (10 μM) at 298 K in aqueous phosphate buffer (pH 7) monitoring the enhanced emission of 4-AC with varying concentrations of β-CD; curves (a−f) represent 0, 8.0, 12.0, 16.0, 20.0, and 28.0 μM AP, respectively; λ_{exc} = 290 nm; inset: variation of singlet-state average lifetime (<τ>) of 4-AC in aqueous buffer monitoring the λ_{exc} of emission with increasing concentration of β-CD. (B) Fluorescence decay of 4-AC (10 μM) at 298 K in aqueous phosphate buffer (pH 7) monitoring the enhanced emission of 4-AC with varying concentrations of γ-CD; curves (a−f) represent 0, 12.0, 18.0, 30.0, 42.0, and 60.0 μM AP, respectively; λ_{exc} = 290 nm; inset: variation of singlet-state average lifetime (<τ>) of 4-AC in aqueous buffer monitoring λ_{exc} of emission with increasing concentration of γ-CD. Excitation and emission band pass = 10 and 5 nm, respectively, in each case of β-CD and γ-CD.

https://doi.org/10.1021/acsomega.0c06152
ACS Omega 2021, 6, 11878−11896

Table 3. Singlet-State Lifetime Data of 4-AC (10 μM) in the Presence of CDs at 298 K

system	$\tau_1(\alpha)$ ns	$\tau_2(\alpha)$ ns	τ_{av} (ns)[a]	χ^2
		α-CD		
0 μM	4.94 (3.34%)	0.85 (96.66%)	0.99	0.96
3 μM	3.98 (3.23%)	0.91 (96.77%)	1.01	0.90
4.5 μM	3.54 (7.09%)	0.84 (92.91%)	1.03	1.01
7.5 μM	3.47 (6.84%)	0.86 (93.16%)	1.04	0.95
9 μM	3.31 (11.16%)	0.79 (88.84%)	1.07	1.02
10.5 μM	3.34 (10.78%)	0.84 (89.22%)	1.11	1.21
		β-CD		
0 μM	4.94 (3.34%)	0.85 (96.66%)	0.99	0.96
8 uM	3.90 (10.12%)	0.80 (89.88%)	1.11	1.23
12 μM	4.15 (12.82%)	0.89 (87.18%)	1.31	1.15
16 μM	3.89 (23.09%)	0.90 (76.91%)	1.59	0.92
20 μM	3.75 (29.63%)	0.92 (70.37%)	1.76	1.28
28 μM	3.89 (37.47%)	1.07 (62.53%)	2.13	1.15
		γ-CD		
0 μM	4.94 (3.34%)	0.85 (96.66%)	0.99	0.96
12 μM	4.56 (12.64%)	0.95 (87.36%)	1.41	1.09
18 μM	4.45 (23.24%)	1.25 (76.76%)	1.99	1.20
30 μM	4.36 (36.21%)	1.30 (63.79%)	2.41	1.07
42 μM	4.29 (38.53%)	1.33 (61.47%)	2.47	1.23
60 μM	4.19 (45.55%)	1.35 (54.45%)	2.64	1.17

[a]Error in the measurements is ±0.1 ns.

major contribution (~97%) and a relatively slower component (~4.94 ns) with very little contribution (~3%) illustrated the presence of free 4-AC molecule and the solvated cluster of the probe 4-AC molecule, respectively. Now, the lifetime values of the 4-AC molecule in the presence of all CD molecules are measured and listed in Table 4. The lifetime decay of the encapsulated 4-AC molecule with β-CD and γ-CD molecules was deconvoluted with the biexponential fitting curve (Figure 6).

Table 4. Singlet-State Lifetime Data of 4-AC (10 μM) in the Presence of Varying Compositions of EG−Water Systems at 298 K

system					
water	EG	$\tau_1(\alpha)$ ns	$\tau_2(\alpha)$ ns	τ_{av} (ns)[a]	χ^2
100	0	4.94 (3.34%)	0.85 (96.66%)	0.99	1.13
80	20	4.31 (5.28%)	0.98 (94.72%)	1.16	1.06
60	40	3.83 (5.73%)	1.02 (94.27%)	1.18	1.22
40	60	3.75 (6.12%)	1.27 (93.88%)	1.42	1.12
20	80	3.68 (6.53%)	1.60 (93.48%)	1.74	1.15
10	90	4.92 (6.72%)	1.74 (93.28%)	1.95	1.24
0	100	4.95 (7.77%)	1.98 (92.23%)	2.21	1.05

[a]Error in the measurements is ±0.1 ns.

The average lifetime value of the 4-AC molecule increase on addition of CD molecules and are consistent with the steady-state fluorescence spectra. For all cases of the complexes of the 4-AC molecule and CD, the biexponential decay of the 4-AC molecule has been portrayed by the slight decrement of the slower component values with an increase in the percent contribution along with the small increase in the faster component with a decrease in its percent contribution (Table 3). These data pointed out the extent of the distribution of the 4-AC molecule in bulk aqueous medium and inside the nanocavity of the CD molecule. Gradual addition of CD molecules increases the percentage contribution of the longer component supporting the stronger inclusion of the guest molecule inside the CD cavity at the expense of the nonradiative decay arising out of intermolecular H-bonding with the solvent molecules, and the relative contribution due to free 4-AC molecule in bulk water decreases progressively in all CD−4-AC complexes (Table 3). The occurrence of a multiexponential decay pattern with the gradual addition of the CD molecules follows the complex trend in all the CD−guest complexes as the guest 4-AC molecule resides in a more or less heterogeneous environment. So, taking into account the average fluorescence lifetime values substantiates the entrapment of the fluorophore inside the nanocavity of the host CD molecules as compared to assessing the individual decay values in all host−guest complexes.

The protective actions by the encapsulation of the guest molecule from the bulk aqueous environment follow a general trend according to the shape and size of the CD molecules. The faster component of lifetime (τ_1) (corresponds to the free 4-AC molecule) illustrated an increased value with an increase in the concentration of all CD molecules; the order of the increment is γ-CD > β-CD > α-CD. For the α-CD−4-AC complex, the host molecule experiences very slight change in the lifetime values (an almost constant value is observed, Table 3), thereby inferring the presence of increased bulk viscosity of the solution inside the host molecules as the cavity size of CD is increased from α-CD to γ-CD. Moreover, the percent amplitude associated with slower component of lifetime values demonstrates that the component of encapsulated guest inside the host molecule shows an increment in a regular fashion with the increased concentration of the host molecule along with the progressive decrement of the unbound probe molecule (Table 3). Now, it is more appropriate to note that the percent contribution of the slower lifetime component (τ_2) follows the order γ-CD > β-CD > α-CD at the saturation level of the encapsulation process, which confirms that the degree of encapsulation is the highest in the cavity of γ-CD and the lowest for α-CD cavity.

The shorter lifetime component values are slightly increasing with the varying concentrations of CD molecules (specially for β-CD and γ-CD) (Table 3), which could be rationalized considering the enhancement of the overall bulk viscosity of the surrounding of 4-AC molecule with the increase in the concentration of the CD molecules. This situation could be explained in the presence of the mixed solvents having almost similar polarity but different viscosities. Fluorescence lifetime values of 4-AC in the presence of mixed solvents comprising different proportions of ethylene glycol (EG) ($E_T(30)$ = 56.3) and water ($E_T(30)$ = 63.1) showed a gradual increment of average lifetime values (Table 4) from the bulk aqueous buffer solution to varying concentrations of EG. The increase in the shorter component lifetime values at higher CD concentrations is thus attributed to the increase in local viscosity around 4-AC and is comparable with the EG−water system and substantiates the fluorescence spectra of 4-AC in the presence of varying percentages of the EG−H_2O mixture (Figure S2). The microviscosity of 4-AC in the presence of the highest concentration of CD molecules is thus nearer to that of the 60:40 water/EG mixture, as observed also from the emission of 4-AC at higher concentrations of 4-AC.

However, the fluorescence quantum yield does not follow the similar trend as observed for the variation in the average lifetime values of the CD−guest complexes (Tables 2 and 3).

https://doi.org/10.1021/acsomega.0c06152
ACS Omega 2021, 6, 11878−11896

This incongruity between the steady-state and time-resolved fluorescence studies could be elucidated by considering the interaction of 4-AC with different polar protic or aprotic solvents (see previous section). The stability of the emissive state of 4-AC was explained by the intermolecular hydrogen-bonding ability of the polar protic solvents resulting in operation of the nonradiative decay channel through formation of H-bond between the heteroatom(s) present in the solvent molecule and the oxygen atom in the polar protic molecules. Generally, an emission profile of a fluorescence probe with a host molecule like CDs could not give any clear picture about the proper fraction of the probe encapsulated within the host and/or the fraction of free probe moving in the bulk aqueous solvent. The encapsulation also renders the hydrophobicity of the probe and motional restriction of the probe inside the host molecules. Hence, the extent of hydrophobicity and motional constraint (due to steady state anisotropy) due to encapsulation could not be judged appropriately by the steady-state fluorescence studies. Time-resolved fluorescence studies for all CD and 4-AC complexes confirm our proposition very well. Molecular docking studies support this contention.

Now, the fluorescence quantum yield (φ_f) and average lifetime values ($<\tau_f>$) of 4-AC are employed to determine the radiative decay rate constant (k_r) and the nonradiative decay rate constant (k_{nr}) for 4-AC emission in the presence of the CD molecules using eqs 1 and 2.

The values of k_r and k_{nr} for all 4-AC−CD systems are tabulated in Table 2. It is obvious that in the bulk aqueous environment, the nonradiative decay rate is higher, and in the presence of the CD molecules, the k_{nr} values decrease strongly, implying the entrapment of the 4-AC molecule in the hydrophobic environment of the CD cavity.

Steady-State Fluorescence Anisotropy Study of 4-AC at 298 K. Steady-state fluorescence anisotropy measurement provides significant idea about the nature of the microenvironment around the fluorescent ligand. It has enormous application potential in the biophysical and biochemical research because factors affecting the size, shape, or segmental flexibility of a molecule will affect the observed anisotropy.[2,3] The degree of restriction imposed by the microenvironment of the fluorophore (ligand/drug) is clearly manifested by the fluorescence anisotropy studies of the ligand/drug with the supramolecular or biomolecular systems, which can be exploited for finding out the probable location of the ligand in different microheterogeneous environments.[2−4,32,46,56,66]

The considerable augmentation of fluorescence anisotropy (r) values of the 4-AC molecule with the progressive addition of three CD systems, viz., α-CD, β-CD, and γ-CD, have been figured out in Figure 4D. These features in all cases allocate the entrapment of the 4-AC molecule in the internal nanocavity of the CD molecules, which clearly put some signature of the existence of the motionally constrained zone of the CD molecules as compared to the free aqueous buffer region. For all CD−4-AC complexes, the limiting levels of saturation of the steady-state anisotropy values (r) are almost similar (∼0.020) (Figure 4D, Table 2), indicating that the judgment about the degree of interaction between the 4-AC and CD molecules with different nanocavities seems to be impossible. The probable reason might be that the overall tumbling motions (major determining factor for the enhancement of the fluorescence anisotropy) of the 4-AC−CD complexes are almost similar with respect to dimension in all three cases.

Binding Constant (K_b) for the Association of the Fluorophore with Supramolecules. Supramolecular system or biomolecular system can protect fluorophore molecules from any kind of external perturbation.[32,56] The confinement in the hydrophobic cavity can lead to changes in various photophysical and photochemical reactivities of the fluorophore, and this strongly depends on the value of the binding constant of the binding of the fluorophore with the supramolecules or biomolecules.

The binding constant (K_b) of the guest 4-AC molecule with the host-organized assemblies or any other supramolecules is estimated by determining the binding constant from the fluorescence intensity of the enhanced emission of the ligand as a function of added concentrations of CD molecules employing modified Benesi−Hildebrand equation[9,67]

$$(F_\infty - F_0)/(F_x - F_0) = 1 + 1/K[L] \quad (4)$$

where, F_0, F_∞, and F_x are the relative fluorescence intensities of the enhanced emission of ligand 4-AC considered in the absence of all CD molecules, at some intermediate concentration of the CD molecules, and at a concentration of complete interaction, respectively, K is the binding constant, and $[L]$ is the concentration of added host CD molecules.

A plot of $(F_\infty - F_0)/(F_x - F_0)$ against $[L]^{-1}$ provides the binding constant (K) from the slope, and the linearity of the plots confirms a 1:1 binding between 4-AC and the CD molecules (Figure 7). The binding constant values and the free energy of binding (ΔG^0) obtained for all three CD complexes at 298 K are listed in Table 2.

Time-Resolved Anisotropy Study of the Ligand 4-AC at 298 K. The time-resolved fluorescence anisotropy is dependent on the rotational diffusion and/or rotational relaxation of the fluorophore in the microenvironment of the supramolecules or biomolecules.[4,9,56] The rotational relaxation of the fluorescence probe is affected when the fluorescence probe goes from the bulk water to the CD environment. Hence, to ensure this, the fluorescence anisotropy decays of the 4-AC molecule in the presence of all CD moieties were measured. The rotational anisotropy decays of 4-AC in all CD−4-AC complexes are measured by monitoring the enhanced emission of 4-AC in the complex with λ_{exc} = 290 nm, and from the fitted curve, the rotational correlation time (θ_c) of 4-AC in all CD molecules is recovered as almost similar values ∼2.0 ns. The recovered single exponential values for all CD−4-AC complexes are summarized in Table 2. Although determination of the θ_c value for the free 4-AC molecule is not possible due to limitation of the detection limit of the instrument, the recovered correlation times for all CD complexes clearly signify the motional inflexibility suffered by the 4-AC molecule due to entrapment of the probe inside the CD cavity (Table 2).

Molecular Docking Studies. The interaction of 4-AC with all CD molecules could be substantiated by molecular docking studies. The docking studies have been carried out with 4-AC provided in Scheme 1. The docked pose of all 4-AC−CD complexes are provided in panel A of Figure 8. The free energy of binding obtained from docking studies of the host−guest complexes is in the following order α-CD > β-CD > γ-CD (Table 5), which is comparable with the free energy of binding obtained from the experimental data for all CD−4-AC complexes. This supports the contention that α-CD is the stronger binding or encapsulating agent than β-CD and γ-CD. The docked structures of all three host−guest complexes illustrate that the azide compound orients itself in a specific

https://doi.org/10.1021/acsomega.0c06152
ACS Omega 2021, 6, 11878−11896

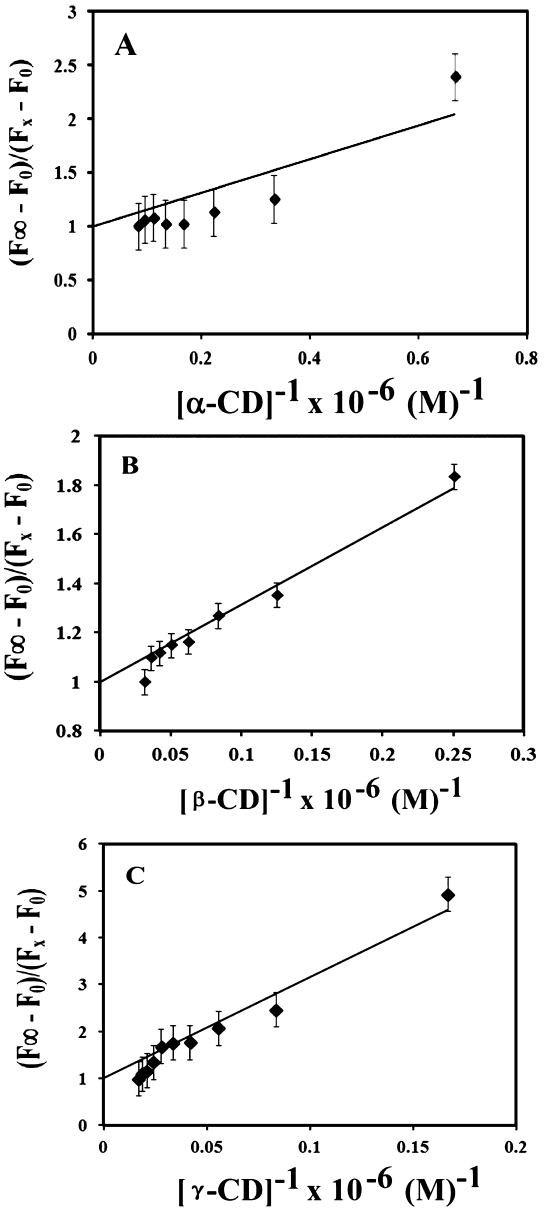

Figure 7. Plot of (A) $[F_\infty - F_0]/[F_x - F_0]$ against $[\alpha\text{-CD}]^{-1}$, (B) $[F_\infty - F_0]/[F_x - F_0]$ against $[\beta\text{-CD}]^{-1}$, and (C) $[F_\infty - F_0]/[F_x - F_0]$ against $[\gamma\text{-CD}]^{-1}$.

direction, with the phenyl part located within the CD cavity and the polar functional part away from the cavity (panel A of Figure 8). CD preferentially encapsulates the more hydrophobic part of the azide compound within its cavity. The orientation of the polar residues of the guest molecule is away from the CD cavity, which indicates that it can interact with the solvent molecules outside the CD cavity. This is in confirmation with the photophysical studies of 4-AC with all CD molecules and also in the presence of different solvent molecules. The experimental results showed that the availability of the nonbonding electrons on the heteroatom of the 4-AC molecule is less due to H-bonding with the −OH group present in the CD molecule, which retards the emission of 4-AC upon excitation with 330 nm. This result could be corroborated by considering the fact that the azide group of the guest molecule is found to associate itself through H-bonding in the case of the γ-CD complex, whereas both N and

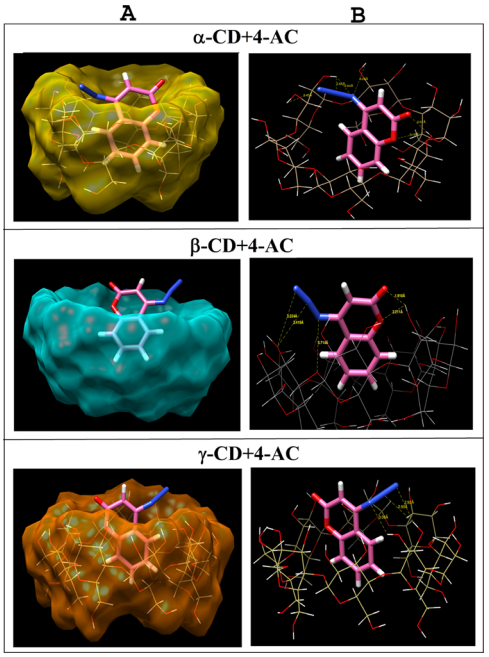

Figure 8. Panel (A) represents the docked pose of 4-AC in the complexes with α-CD, β-CD, and γ-CD, respectively. Panel (B) represents H-Bonding distances between ligand atoms and different atoms of CD molecules of the docked complexes.

Table 5. H-Bonding Distances Between the Ligand Atom and Different Atoms of the CD Molecules of the Docked Complexes

system	ligand atom	CD atom	distance (Å)	ΔG^0 (Kcal mol^{-1})
α-CD−4AC	N14	C3-OH	2.43	−4.7
	N13	C2-OH	2.69	
	N12	C2-OH	2.64	
	N12	C3-OH	3.25	
	O10	C3-OH	3.12	
	O11	C3-OH	2.01	
β-CD−4AC	N14	C3-OH	3.32	−4.1
	N13	C3-OH	3.42	
	N12	C1-O (glycosidic O)	3.71	
	O10	C2-OH	3.21	
	O11	C2-OH	1.91	
	N14	C3-OH	2.92	−3.8
	N13	C3-OH	2.93	
γ-CD−4AC	N12	C2-OH	3.00	
	O11	C3-OH	3.21	

O of the azide compound participate in H-bonding with the host for α-CD and β-CD (Panel B of Figure 8, Table 5). The number of H-bonding formed between the host and the guest is maximum for α-CD and minimum for γ-CD, which suggests that the H-bonding interaction plays a significant role in stabilizing the host−guest complex (panel B of Figure 8, Table 5). The fluorescence quantum yield as well as the binding constant data of the CD−4-AC complexes support this result obtained from molecular docking studies, although the time-resolved studies of CD−4-AC complexes generate a divergence, which might be due to the interplay between the photophysical dynamics of 4-AC−CD complexes and the solvation dynamics of the 4-AC-solvent (here aqueous buffer) operational in our case.

https://doi.org/10.1021/acsomega.0c06152
ACS Omega 2021, 6, 11878−11896

In Biomolecular Systems. *Steady-State Absorption and Fluorescence Studies Monitoring Ligand Emission at 298 K.* The absorption spectra of free 4-AC (10 μM) and 4-AC (10 μM) in the presence of BSA (5 μM) in aqueous medium at 298 K are provided in e Figure S3. Similar spectra for 4-AC (10 μM) are observed in the presence of HSA. With the addition of SAs, the absorbance is found to decrease to a small extent, with no significant shift in λ_{max} (Figure S3), which indicates incorporation of the ligand 4-AC in the protein pocket.

The emission spectra of 4-AC are also modified in the presence of SAs, similar to that in the CDs. Figure 10

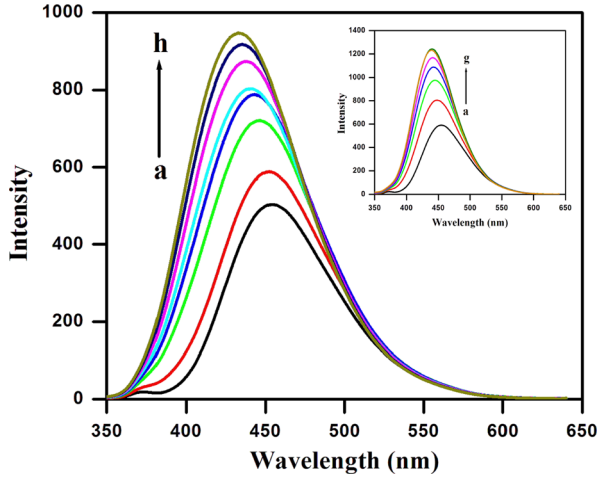

Figure 9. Fluorescence spectra of 4-AC (10 μM) at 298 K with varying concentrations of BSA; curves (a−h) represent 0, 0.030, 0.091, 0.125, 0.152, 0.182, 0.244, and 0.303 μM BSA, respectively; λ_{exc} = 330 nm; excitation and emission band pass = 10 and 5 nm, respectively. Inset: Fluorescence spectra of 4-AC (10 μM) at 298 K with varying concentrations of HSA; curves (a−g) represent 0, 0.071, 0.143, 0.200, 0.278, 0.345, and 0.417 μM HSA, respectively; λ_{exc} = 330 nm; excitation and emission band pass = 10 and 5 nm, respectively.

demonstrates the emission spectra of ligand 4-AC in aqueous buffer solution as a function of increasing concentrations of SAs with λ_{exc} = 330 nm at 298 K. There has been a steady increase in the emission of 4-AC with an appreciable blue shift of the emission maxima of the ligand in the presence of proteins (Figure 9). The quantum yield (φ_D) of the enhanced emission of the ligand increases approximately 1.5 times in the complex with BSA and 2.1 times in the complex with HSA as compared to that of pure ligand in the same aqueous buffer (pH 7) (Table 6, Figure S4IA,B). The blue shift of the emission maxima of the ligand from ∼452 nm (free ligand) to ∼434 nm (for BSA) and ∼438 nm (for HSA) with increasing protein concentrations suggests that the ligand molecule experiences a less polar or more hydrophobic environment in both the SA−ligand complexes as compared to the free ligand.

Figure S4IIA,B represents the variation of fluorescence anisotropy (r) of emission of ligand 4-AC as a function of protein concentration for both the SAs. The steady-state anisotropy (r) value in aqueous buffer solution is 0.03 (Table 6). In the presence of SAs, the anisotropy values gradually increase with an increase in the protein concentration and then reaches a saturation value (0.164 for BSA and 0.191 for HSA) (Figure S4IIA,B, Table 6). This implies enhanced degree of motional restriction imposed on the ligand in the micro-environment of the proteins. In the case of HSA, a higher value

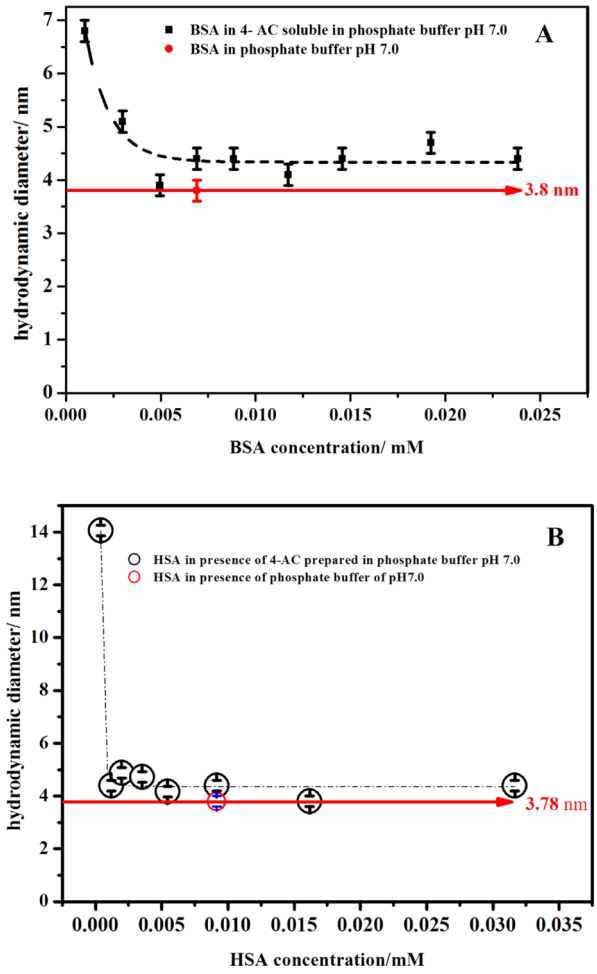

Figure 10. Change in hydrodynamic diameter of (A) BSA and (B) HSA in the presence and absence of 4-AC prepared in phosphate buffer of pH 7.0. The red line represents the average value of hydrodynamic diameter of free BSA in phosphate buffer of pH 7.0. Error bars are given to each experimental point. The standard deviation of hydrodynamic diameter is ±0.2 nm.

of anisotropy at the saturation concentrations (Table 6) indicates that the probe molecule is experiencing a somewhat more rigid environment in the core of HSA, which indicates a greater binding of the 4-AC molecule in the HSA environment than that in the BSA environment (see the next section). Though these observations are in good agreement with the fluorescence quantum yield as well as fluorescence lifetime data, the binding constant values determined are in contradiction. This observation can be rationalized considering some specific interactions such as hydrogen bonding centered around the protein and the heteroatoms present in the ligand molecules, leading to some additional restriction imposed on the motion of the overall molecule or trapping of the probe in some motionally constrained site such as the cleft or crevice of the protein. Some steric constrain may also play a role in fixing the spatial orientation of the probe molecule.[68] Molecular docking studies also help to get a clear vision of this observation (see the next section).

The bindings between SAs and 4-AC are analyzed by determining the binding constant from the fluorescence intensity of enhanced emission of ligand as a function of added protein concentration employing modified Benesi−Hildebrand equation (eq 4)[9,67] with the linear plot (Figure

https://doi.org/10.1021/acsomega.0c06152
ACS Omega 2021, 6, 11878−11896

Table 6. Singlet-State Lifetime and other Photophysical Parameters of 4-AC Monitored at the Enhanced Emission in Aqueous Buffer (pH 7) and in Serum Albumins at 298 K

system	λ_{max} [a] (nm)	quantum yield (φ_f)	$\tau_1(\alpha)$ ns	$\tau_2(\alpha)$ ns	τ_{av} (ns) [b]	χ^2	steady state anisotropy (r)	rotational correlation time (θ_c) (ns)	rate of the radiative transition ($k_r \times 10^{-7}$) (s^{-1})	rate of the non-radiative transition ($k_{nr} \times 10^{-8}$) (s^{-1})
free 4-AC (10 μM)	453.2	0.056	0.64 (100%)		0.64	1.16	0.030		8.8	14.75
+0.030 μM BSA	451.6	0.057	0.63 (85.88%)	1.13 (14.12%)	0.70	1.05	0.012			
+0.059 μM BSA	446.0	0.067	0.63 (85.87%)	2.96 (14.13%)	0.96	1.17	0.077			
+0.091 μM BSA	443.0	0.071	0.64 (82.35%)	3.21 (17.65%)	1.09	1.33	0.083			
+0.125 μM BSA	440.4	0.074	0.63 (74.35%)	3.21 (25.65%)	1.29	1.13	0.103			
+0.152 μM BSA	437.8	0.076	0.63 (70.95%)	3.28 (29.05%)	1.40	1.07	0.121			
+0.182 μM BSA	435.6	0.075	0.64 (68.88%)	3.35 (31.12%)	1.48	1.22	0.134			
+0.244 μM BSA	433.0	0.084	0.64 (60.85%)	3.36 (39.15%)	1.70	1.12	0.148			
+0.303 μM BSA	434.2	0.088	0.57 (57.83%)	3.39 (42.17%)	1.76	1.04	0.164	2.7	5.0	5.18
+0.071 μM HSA	448.2	0.078	0.64 (94.52%)	2.32 (5.48%)	0.73	1.21	0.060			
+0.143 μM HSA	444.2	0.094	0.64 (90.72%)	3.14 (9.28%)	0.87	1.20	0.091			
+0.200 μM HSA	442.0	0.104	0.63 (79.75%)	3.74 (20.25%)	1.26	1.17	0.126			
+0.278 μM HSA	441.4	0.112	0.64 (74.88%)	3.70 (25.12%)	1.41	1.15	0.144			
+0.345 μM HSA	439.8	0.120	0.63 (68.57%)	3.69 (31.43%)	1.59	1.20	0.159			
+0.417 μM HSA	438.4	0.123	0.64 (64.43%)	3.70 (35.57%)	1.73	1.21	0.183			
+0.476 μM HSA	438.0	0.123	0.64 (62.39%)	3.78 (37.61%)	1.82	1.13	0.195			
+0.556 μM HSA	437.9	0.120	0.64 (61.05%)	3.81 (38.95%)	1.87	1.17	0.191	3.2	6.4	4.71

[a] λ_{exc} = 375 nm. [b] Error in the measurements is ±0.1 ns.

https://doi.org/10.1021/acsomega.0c06152
ACS Omega 2021, 6, 11878−11896

S5), and the binding constant values obtained for BSA and HSA at 298 K are 9.80×10^6 and 7.02×10^6 M^{-1}, respectively, with the binding site $n = 1$ for both the cases.[9]

Time-Resolved Fluorescence Studies at 298 K. The singlet-state lifetime of the ligand 4-AC is measured in both the SAs by monitoring the enhanced emission of the ligand. The decay of emission of the ligand in aqueous buffer (pH 7) is best fitted with a single exponential, and the lifetime recovered is 0.64 ns (100%) (Table 6). The lifetime of the ligand 4-AC is also measured as a function of the added concentration of BSA and HSA by monitoring the enhanced emission maxima in each case using λ_{exc} = 375 nm (Table 6). The representative decay profiles are presented in Figure S6. The decays were best fitted with two components where χ^2 is found to be close to 1 in each case on addition of BSA and HSA (Table 6). The biexponential decays are estimated with a lifetime component close to that of the free ligand in aqueous buffer (~0.64 ns) and another component of increased lifetime (~1.12−3.39 ns for BSA and ~2.32−3.81 ns for HSA) (Table 6). The relative contribution of the shorter component decreases gradually with a simultaneous increase of the contribution of the longer component for both the protein−ligand systems (Table 6). Hence, the increased lifetime values in both the protein−ligand complexes suggest the more rigid environment than the ligand 4-AC experiencing gradually upon binding with the protein. The average lifetime increases to 1.76 ns in BSA and 1.87 ns in HSA (Figure S4IIIA,B, Table 6) compared to 0.64 ns for free ligand in aqueous buffer with the gradual increase in the concentration of SAs, which are consistent with the steady-state fluorescence data (Table 6).

The time-resolved fluorescence anisotropy is dependent on the rotational diffusion and/or rotational relaxation of the fluorophore in the microenvironment of the proteins. The anisotropy decays of 4-AC in both the SA−ligand complexes are measured by monitoring the enhanced emission of 4-AC in the complex with λ_{exc} = 375 nm, and from the fitted curve, the rotational correlation times (θ_c) of 4-AC in BSA and HSA are recovered as 2.7 and 3.2 ns. There is an increased value of θ_c of 4-AC in the presence of the microenvironments of the SAs (Table 6). Table 6 clearly demonstrates the rotational restriction experienced by the ligand molecule. The binding constant of the 4-AC−HSA complex is less than that of the 4-AC−BSA complex, and the larger θ_c value in HSA indicates more rotational restriction of 4-AC in the presence of HSA compared to that in BSA.

The decrease of the polarity around the ligand 4-AC in the microenvironment of SAs might be elucidated by calculating the radiative (k_r) and nonradiative rate constants (k_{nr}) (Table 6) calculated using eqs 2 and 3. The reduction in the nonradiative rate constants data of the ligand in the proteineous environments supports the rigidity of the micro-environment, and hence there is an increase of θ_c value compared to that of the free buffer medium.

Molecular Docking Studies. Molecular docking studies are employed to determine the probable location of the drug molecule in the binding pocket of the protein molecule and also the microenvironment of the ligand before and after complexation of the protein by the experimental findings in the SA−ligand complexes. The best docking pose of the protein−ligand complexes could be directly correlated with the experimental findings by considering the minimum score in the FlexX run for both the complexes of BSA and HSA,[6] which supports the stronger binding of the ligand 4-AC for BSA in the complexes than that for HSA, as evidenced in the binding constants data. Docking studies show that the ligand (4-AC) binds close to site I in domain II in both cases of BSA and HSA but with somewhat higher binding affinity in the case of the latter protein.

The present experimental studies of the enhancement of the ligand by the interaction of 4-AC with the biomolecular systems to get the idea about the microenvironment of the ligand could be judged in a different approach than that in our earlier study[6] of fluorescence quenching studies.

(i) Consideration of the Accessible Surface Area of the Ligand Atoms. This is much more prominent in the case of BSA than HSA, suggesting that the ligand becomes almost shielded by the amino acid residues in the former protein (Table 7). In both the cases O10, O11, and N14 show

Table 7. Change in the ASA (Å) of Different Atoms of Ligand 4-AC in Both Complexes of BSA and HSA

	free 4-AC	4-AC−BSA		4-AC−HSA	
atom no.	ASA (Å^2)	ASA (Å^2)	ΔASA (Å^2)	ASA (Å^2)	ΔASA (Å^2)
C1	22.834	0.054	22.780	2.838	19.996
C2	22.857	0.929	21.928	12.698	10.159
C3	17.486	1.051	16.435	9.763	7.723
C4	3.833	0	3.833	1.741	2.092
C5	7.521	0	7.521	1.467	6.054
C6	20.961	0	20.961	0	20.961
O10	14.393	0	14.393	0.928	13.465
C7	5.728	0	5.728	0.753	4.975
C8	15.316	0	15.316	0	15.316
C9	14.945	0	14.945	1.852	13.093
N12	18.597	0	18.597	2.211	16.386
N13	14.121	0	14.121	0.739	13.382
N14	63.986	1.35	62.636	6.496	57.49
O11	42.853	0	42.853	1.079	41.774
	285.431	3.384	**282.047**	42.565	**242.866**

maximum change in the accessible surface area (ΔASA) value, which indicates that electrostatic interaction may play a key role in protein−ligand interaction, thereby bringing these electronegative atoms close to the amino acid residues. Hence, the larger binding constant values for the BSA−4-AC complex compared to those for the HSA−4-AC complex determined experimentally by different methods could be addressed for involvement of different atoms by the change in their ASA values in the complexes.

(ii) Consideration of the Change in the ASA of Different Amino Acids due to Binding. Our previous studies[6] of protein−ligand docking studies on 4-AC−SA complexes show the different amino acid residues present within 5 Å of the ligand 4-AC. The ASA values provided in our earlier work[6] have been considered in another approach to establish the constrained environment around the ligand. Table 8 shows the different residues of SAs which change in ASA (Å^2) values upon binding with 4-AC. It is noticed that a greater number of polar residues (Lys 195, Trp 214, Arg 218, and Asp 451) have a higher ΔASA value for HSA, whereas only two polar residues (Trp 213 and Asp 450) become highly shielded in the case of BSA (Table 8). Also, the residues which lose over 10 Å^2 in their ASA values upon binding with the ligand 4-AC are accountable in the binding process. It has been observed that six residues, viz., Lys 195, Trp 214, Arg 218, Pro 447, Asp 451, and Val 455, lose over 10 Å^2 in their ASA values in the binding

https://doi.org/10.1021/acsomega.0c06152
ACS Omega 2021, 6, 11878−11896

Table 8. Changes in the ΔASA(Å^2) of the Amino Acid Residues of Docked Complexes of BSA and HSA with 4-AC

BSA−4-AC[a]		HSA−4-AC[a]	
amino acid residues	ΔASA (Å^2)	amino acid residues	ΔASA (Å^2)
Arg 194	11.98	Lys 195	32.34
Leu 197	24.22	Leu 198	8.11
Arg 198	6.31	Trp 214	14.52
Ser 201	5.76	Arg 218	17.63
Leu 210	1.13	Val 343	2.22
Trp 213	28.4	Val 344	1.62
Arg 217	7.34	Pro 447	10.76
Val 342	8.5	Cys 448	7.23
Ser 343	8.86	Asp 451	17.55
Leu 346	6.64	Tyr 452	7.36
Asp 450	17.34	Ser 454	1.82
Ser 453	7.6	Val 455	10.92
Leu 454	5.47		
Leu 480	13.64		
total (including all residues)	**153.72**	**total** (including all the residues)	**132.65**

[a]Underline residues are polar residues.

of the ligand in the HSA−4-AC complex, whereas five residues, viz., Arg 194, Leu 197, Trp 213, Asp 450, and Leu 480 lose over 10 Å^2 in their ASA values in the BSA−4-AC complex (Table 8). This clearly indicates that the ligand molecule is situated in more constrained environments of HSA than in BSA, though the binding constant is greater for BSA than that for HSA. Hence, the anisotropy as well as the θ_c value monitoring the enhanced emission of the ligand is more for the HSA−4-AC complex as compared to the BSA−4-AC complex (Table 6).

(iii) Consideration of the Effect of H-Bonding Between Different Atoms. The atoms involved in H-bonding are obtained from the structure analysis tool in Chimera software.[6] It is observed that for the BSA−4-AC complex, three Arg residues are involved in H-bonding, whereas for the HSA−4-AC complex, only one Arg residue is involved in the binding process. The polarity of the Trp environment might be increased due to the presence of an Arg residue near a Trp residue due to the charge of the Arg side chain, the formation of a hydrogen bond of one of the NH groups on the Arg side chain with the indole ring, or the interaction through a NH−π bond with the indole ring.[69−71] This definitely confirms the greater motional restriction of 4-AC in the microenvironment of HSA as compared to BSA, thereby making θ_c value more for the HSA−4-AC complex as compared to the BSA−4-AC complex (Table 6).

DLS Measurement. DLS measurements have been carried out to investigate the hydrodynamic diameters (R_H) of free SAs and the complexes of SAs with 4-AC. The average hydrodynamic diameter (R_H) of free BSA (within the concentration range of 9.9×10^{-4} to 0.02 mM) and HSA (within the concentration range of 4.01×10^{-4} to 0.03 mM) in the presence of phosphate buffer of pH 7.0 is found to be 3.80 and 3.78 nm, respectively (Figure 10). The values obtained for free BSA and HSA are in good agreement with that of the earlier data.[72,73] In the presence of 4-AC (10 μM), the R_H values of both BSA and HSA are found to be greater than their corresponding average values in their free states and have been shown in the plot of R_H values against the concentration of SAs (Figure 10). Representative diagram comprises % intensity versus size (nm) plots of BSA in the presence and absence of 4-AC, as shown in Figure S7. Also, the low polydispersity index values found in this present study suggest that monodispersing solutions have been formed due to complexation of BSA/HSA at all concentrations with 4-AC (data not shown). The differences in the diameter in the free state and those in presence of 4-AC are increased at a low concentration of both BSA and HSA (at 9.9×10^{-4} mM for BSA and 4.01×10^{-4} mM for HSA), respectively, and the value is somewhat higher in the case of complex of HSA (R_H = 14.06 nm) than that of BSA (R_H = 6.8 nm). Initially. a small addition of BSA/HSA to 10 μM 4-AC significantly increases the hydrodynamic diameter compared to their radii in their free state due to unfolding of native SA structures influenced by the ligand. This influence was greater in the case of HSA compared with BSA, manifested in R_H values at a low concentration of proteins. However, with the gradual augmentation of concentration of both BSA/HSA, the hydrophobicity of the immediate medium of 4-AC increases, leading to a decrease in the effective distance of 4-AC-Trp residue(s) (less hydrodynamic diameter). This phenomenon supports the observation of gradual increase of lifetime values as well as the increased fluorescence quantum yield values of the ligand upon gradual addition of BSA/HSA. After a particular concentration (for 0.005 mM BSA and for 0.002 mM HSA), there is no significant change in the hydrodynamic diameter. This is probably due to the occurrence of the dynamic equilibrium between the bound and free 4-AC ligands, which is manifested in the saturation of fluorescence intensity at a high concentration of BSA/HSA.

CONCLUSIONS

The present work demonstrates the interaction of the ligand 4-AC with some biomimicking systems, viz., α-CD, β-CD, and γ-CD, and biomolecular systems, BSA and HSA, by steady-state and time-resolved fluorescence studies and also steady-state and time-resolved fluorescence anisotropy studies by monitoring the enhanced emission of bound 4-AC at 298 K and molecular docking studies. Categorically, these two kinds of systems reveal the following:

1. 4-AC binds strongly with the respective systems with binding constants of the order of 10^5 and 10^6 M^{-1} for CDs and SAs, respectively, at a single binding site.
2. The quantum yield of enhanced emission of 4-AC observed around ∼452 nm in aqueous buffer (pH 7) is markedly enhanced in the presence of CD molecules and BSA/HSA along with the hypochromic shift of the ligand in presence of the proteins. The variation of the quantum yield values is somewhat due to the polarity responsive environment around 4-AC.
3. The lifetime values evidently follow the general trend as in quantum yield for the SA−ligand complexes. For the α-CD−4-AC complexes, the lower viscosity due to the smaller cavity size of α-CD−4-AC produces almost unchanged values of the lifetime for the encapsulated host−guest complexes, thereby differentiating from that of the β-CD and γ-CD complexes with 4-AC. This contention could be rationalized by the emission study of 4-AC in the EG−water mixed solvent system having different viscosities.
4. The variation in the emission maxima, the quantum yield values, and the lifetime of the 4-AC molecule in

https://doi.org/10.1021/acsomega.0c06152
ACS Omega 2021, 6, 11878−11896

different polar protic and aprotic solvents are found to depend on the polarity as well as hydrogen bonding ability of the solvents with the 4-AC molecule. This governs to predict the nature of the environment of 4-AC in binding with the CDs and the protein molecules.

5. The rotational correlation time (θ_c) obtained from the time-resolved anisotropy study in the complexes of 4-AC−CDs and 4-AC−SAs matches well with that calculated from the steady-state anisotropy data. The significant enhancement of the 4-AC emission in both kinds of the confined medium is thus ascribed to the motional restriction of the probe induced by the binding sites of the host molecules.

6. The H-bonding interactions between 4-AC and CD molecules obtained from the molecular docking studies are substantiated to visualize the nature of the microenvironment around the ligand in all CD−4-AC complexes. Also the change in the ASA value and polar contacts/H-bonding distances obtained from molecular docking studies for SA−4-AC complexes support the larger θ_c for 4-AC in the microenvironment of HSA as compared to BSA.

7. The change in hydrodynamic diameter upon ligand binding calculated from the DLS data helps to understand the changes in the microenvironment in the core of SAs due to complexation of 4-AC with SAs.

Thus, these searching and finding investigations by both experimental and theoretical approaches for the biomimetic and biomolecular systems having the altering micro−heterogeneous environments help us to visualize the preliminary steps of finding the drug designing and drug delivery study of the modern pharmaceutical and/or biophysical research endeavor.

EXPERIMENTAL SECTION

Materials and Methods. *Materials.* All analytical grade reagents, chemicals, and CDs (α-CD, β-CD, and γ-CD) and SAs (BSA and HSA) were purchased from Sigma-Aldrich Chemicals Pvt. Ltd. All spectral grade solvents such as DOX, DMSO, ACN, PhCN, *i*-PrOH, EtOH, MeOH, and EG were dried by standard procedures. Aqueous phosphate buffered solution of pH 7 was prepared in triple distilled water for making the experimental solutions.

Instrumentation. *Steady-State Measurements at 298 K.* UV−vis absorption spectra at 298 K were performed using a Hitachi U-2910 spectrophotometer. Steady-state fluorescence measurements at 298 K were carried out with a stoppered cell of 1 cm path length using a Hitachi Model F-7000 spectrofluorimeter equipped with a 150-W xenon lamp. The excitation and emission band passes in all measurements of emission of 4-AC on excitation at 290 and 330 nm were considered as 10 and 5 nm, respectively. Also, the fluorescence quantum yield was determined in each case by comparing the corrected emission spectrum of the systems with those of tryptophan (φ_D = 0.13) and quinine sulfate (φ_D = 0.54) in 0.1 N H_2SO_4, considering the total area under the emission curve.[74]

The steady-state anisotropy (r) was also performed in a Hitachi Model F-7000 spectrofluorimeter with a manual Glen Thompson polarizer and is defined by[74]

$$r = (I_{VV} - G \times I_{VH})/(I_{VV} + 2G \times I_{VH}) \quad (5)$$

$$G = I_{HV}/I_{HH} \quad (6)$$

where I_{VV} and I_{VH} are the emission intensities collected with the samples when the excitation polarizer was orientated vertically and the emission polarizer was oriented vertically and horizontally, respectively. The G factor is defined as the correction factor of the instrument and was determined by keeping the horizontal position with the excitation polarizer and the vertical and horizontal positions with the emission polarizer, respectively.

Time-Resolved Emission Studies at 298 K. Singlet-state lifetime was measured by a Time Master fluorimeter from Photon Technology International (PTI, USA) with a TCSPC set up (PTI, USA) using interchangeable sub nanosecond pulsed LEDs and pico-diode lasers (Picoquant, Germany) and a pulsed laser driver, that is, PDL-800-B (from Picoquant, Germany). All acquisition modes and data analysis of the Time Master system were controlled by the software Felix 32.[75] A pulsed LED PLS-290 (pulse width-600 ps) and a diode laser LDH-375 (pulse width-80 ps) with a repetition frequency of 10 MHz were used for the excitation of 10 μM 4-AC with varying concentrations of CDs and SAs. Instrument response function was measured at the respective excitation wavelength, namely, 290 and 375 nm, using slits with a band pass of 3 nm using Ludox as the scatterer. The decay analyses were carried out by a nonlinear iterative fitting procedure based on the Marquardt algorithm using the deconvolution technique, and intensity decay curves were fitted as a sum of exponential terms.[2,3]

$$F(t) = \sum \alpha_i \exp(t/\tau_i) \quad (7)$$

where α_i represents the pre-exponential factor to the time-resolved decay of the component with a lifetime τ_i. The quality of fit has been assessed over the entire decay, including the rising edge, and tested with a plot of weighted residuals and other statistical parameters, for example, the reduced χ^2 ratio and the Durbin−Watson parameters.[74] The amplitude-weighted average lifetime $\langle\tau\rangle$ was calculated using the equation.[2,3]

$$\langle\tau\rangle = \sum \alpha_i\tau_i / \sum \alpha_i \quad (8)$$

Time-resolved anisotropy decay $[r(t)]$ measurements were also carried out in TCSPC from PTI, USA using a motorized Glen Thompson polarizer and is defined as

$$r(t) = [I_{VV}(t) - G \times I_{VH}(t)]/[I_{VV}(t) + 2 \times G \times I_{VH}(t)] \quad (9)$$

$$G = I_{HV}(t)/I_{HH}(t) \quad (10)$$

where $I(t)$ terms are defined as the intensity decay of emission of 4-AC with excitation polarizer orientated vertically and the emission polarizer oriented vertically and horizontally and G is the correction term for the relative throughput of each polarization through the emission optics. The entire data analysis was carried out with the software Felix 32 which analyses the raw data I_{VV} and I_{VH} simultaneously by global multiexponential program, and then the deconvolved curves (ID_{VV} and ID_{VH}) are used to construct $r(t)$, and from the fitted curve, the rotational correlation time (θ_c) can be recovered.[75]

Docking Studies. *For 4-AC−CD Complexes.* The three-dimensional structure of the azo molecule has been prepared and optimized using Avogadro Software.[76] The three-dimensional structures of α, β, and γ-CD were extracted from the

https://doi.org/10.1021/acsomega.0c06152
ACS Omega 2021, 6, 11878−11896

following PDB files, respectively: 4FEM,[77] 1BFN,[78] and 5E70[79] followed by optimization using Avogadro software.

The docking study of azo with α-, β-, and γ-CD was carried out using AutoDockVina[80] with the grid size 16 Å × 20 Å × 18 Å with the center at coordinate $x = -22.274$, $y = -28.712$, and $z = -18.375$ for α-CD, 34 Å × 32 Å × 34 Å with the center at coordinate $x = -26.594$, $y = -29.781$, and $z = -12.635$ for β-CD, and 44 Å × 37 Å × 26 Å with the center at coordinate $x = 81.717$, $y = 76.619$, and $z = 60.879$ for γ-CD. The structure corresponding to the most negative ΔG (free energy) was selected and analyzed using UCSF Chimera software.[81]

For 4-AC−SA Complexes. The crystal structures of BSA (PDB ID: 4F5S) and HSA (PDB ID: 1AO6) were obtained from Protein Data Bank.[82] The three-dimensional ligand molecule was generated in Sybyl 6.92 (Tripos Inc., St. Louis, USA), and its energy-minimized conformations were obtained using Tripos force field and Gasteiger−Hückel charges with a gradient of 0.005 kcal/mol with 1000 iterations. The protein structure was initially taken followed by removal of water molecules from the pdb structure and addition of polar hydrogens to it. For docking purpose, the whole protein was selected and FlexX software, which is a part of the Sybyl suite, was used for docking of the ligand to the SAs. Based on the free energy of binding (ΔG) of the protein−ligand complex, a series of solutions were generated of various ranks with a particular score.[83] For both the proteins, the structure corresponding to the minimum score was selected and used for further studies. In order to visualize the docked conformations and evaluate the protein−ligand interaction, UCSF Chimera software was used.[81]

ASA Calculations. The solvent exposure of the protein residue was calculated by using *NACCESS* software.[84] In order to estimate the change in the solvent ASA (ΔASA), the difference between the ASA of the free protein, the free ligand, and the protein-bound ligand was calculated for the entire protein and also individual residues using the following equation

$$\Delta\mathrm{ASA}_i = \mathrm{ASA}_{\text{free BSA/free HSA}} - \mathrm{ASA}_{\text{BSA-ligand/HSA-ligand complex}} \quad (11)$$

$$\Delta\mathrm{ASA}_j = \mathrm{ASA}_{\text{free ligand}} - \mathrm{ASA}_{\text{ligand-BSA/ligand-HSA complex}} \quad (12)$$

The change in the ASA of the ith residue of BSA or HSA and jth atom of the ligand is represented by eqs 11 and 12, respectively.

DLS Measurement. DLS measurements were carried out on a Nano ZS Zetasizer (Malvern, UK) with a He−Ne laser (λ = 632.8 nm) at 90° scattering angle at 298.15 K. Different concentration sets of BSA and HSA were incubated with 4-AC (10 μM) for 10 h. The samples were well sonicated for 20 min at low temperature and were filtered through 0.22 and 0.02 mm Whatman syringe filters to a quartz DLS cell of 1 cm path length. 1 mL of solution was taken for each measurement. The measurement of each set of different concentrations of BSA/HSA, both in the presence and absence of 4-AC, was performed three times with an average of 20 measurement runs.

■ ASSOCIATED CONTENT

Supporting Information

The Supporting Information is available free of charge at https://pubs.acs.org/doi/10.1021/acsomega.0c06152.

Plot of Stokes shift (Δ) (cm^{-1}) versus eq 1 for solvents of different polarities; emission spectra of 4-AC in varying percentages (V/V) of water and EG mixed solvent at 298 K; absorption spectra of 4-AC in BSA and in HSA at 298 K; variation of fluorescence quantum yield (Φ_F), fluorescence anisotropy (r), and singlet-state average lifetime (s) of 4-AC in aqueous buffer by monitoring the enhanced emission with increasing concentration of BSA and HSA; plot of $[F_\infty - F_0]/[F_x - F_0]$ against $[\mathrm{BSA}]^{-1}$ and against $[\mathrm{HSA}]^{-1}$; fluorescence decay of 4-AC (10 μM) at 298 K in aqueous buffer (pH 7) in BSA and in HSA; and intensity (%) versus size (nm) plot of BSA (in buffer solution of pH 7.0) in the presence and absence of 4-AC (PDF)

■ AUTHOR INFORMATION

Corresponding Authors

Pinki Saha Sardar − *Department of Chemistry, The Bhawanipur Education Society College, Kolkata 700020, India*; Phone: +91-9830431792; Email: pinkish12@gmail.com, pinki.sahasardar@thebges.edu.in

Anjoy Majhi − *Department of Chemistry, Presidency University, Kolkata 700 073, India*; orcid.org/0000-0003-0142-4940; Phone: +91-7596900172; Email: anjoy.chem@presiuniv.ac.in; Fax: +91-33-1077 2241-3893

Authors

Sandip Paul − *Department of Chemistry, Presidency University, Kolkata 700 073, India*

Pritam Roy − *Department of Chemistry, Indian Institute of Technology, Kharagpur 721302, India*

Sourav Das − *Centre for Surface Science, Physical Chemistry Section, Department of Chemistry, Jadavpur University, Kolkata 700032, West Bengal, India*

Soumen Ghosh − *Centre for Surface Science, Physical Chemistry Section, Department of Chemistry, Jadavpur University, Kolkata 700032, West Bengal, India*; orcid.org/0000-0001-7628-5768

Complete contact information is available at: https://pubs.acs.org/10.1021/acsomega.0c06152

Notes

The authors declare no competing financial interest.

■ ACKNOWLEDGMENTS

A.M. acknowledges the SERB for research grant (ref: EEQ/2019/000194 and SB/FT/CS-188/2012) and the UGC for research grant [F. 30-19/2014 (BSR), F.D. Dy. no. 2161]. S.P. thanks the CSIR, India for his fellowship (award letter no-08/155(0051)/2017-EMR-1, dated-4/12/2017). S.D. acknowledges the CSIR, India for financial assistance. S.G. thanks the UGC CAS of the Department of Chemistry, Jadavpur University, India. P.S.S. acknowledges The Research and Publication Cell, The Bhawanipur Education Society College, Kolkata for funding the Research Grant (grant no.: BESC/RPC/2019-2020/SCI/03). The authors are extremely appreciative of the Presidency University, Kolkata for providing

FRPDF research grant, instrument, and laboratory facilities. The authors are also thankful to the editors and the reviewers of the journal for their valuable comments and suggestions.

REFERENCES

(1) Gopidas, K. R.; Kamat, P. V. Photophysics and photochemistry of phenosafranin dye in aqueous and acetonitrile solutions. *J. Photochem. Photobiol., A* **1989**, *48*, 291−301.
(2) Lakowicz, J. R. *Principles of Fluorescence Spectroscopy*; Kluwer/Plenum Press: New York, 2006, Chapter 17.
(3) Lakowicz, J. R.; Cherek, H. Resolution of Heterogeneous Fluorescence from Proteins and Aromatic Amino Acids by Phase-sensitive Detection of Fluorescence. *J. Biol. Chem.* **1981**, *256*, 6348−6353.
(4) Mukherjee, M.; Sardar, P. S.; Ghorai, S. K.; Samanta, S. K.; Roy, A. S.; Dasgupta, S.; Ghosh, S. Interaction of multitryptophan protein with drug: An insight into the binding mechanism and the binding domain by time resolved emission, anisotropy, phosphorescence and docking. *J. Photochem. Photobiol., B* **2012**, *115*, 93−104.
(5) Sardar, P. S.; Samanta, S.; Maity, S. S.; Dasgupta, S.; Ghosh, S. Energy Transfer Photophysics from Serum Albumins to Sequestered 3-Hydroxy-2-Naphthoic Acid, an Excited State Intramolecular Proton-Transfer Probe. *J. Phys. Chem. B* **2008**, *112*, 3451−3461.
(6) Paul, S.; Sepay, N.; Sarkar, S.; Roy, P.; Dasgupta, S.; Saha Sardar, P.; Majhi, A. Interaction of serum albumins with fluorescent ligand 4-azido coumarin: spectroscopic analysis and molecular docking studies. *New J. Chem.* **2017**, *41*, 15392−15404.
(7) Hansen, J. E.; Pines, E.; Fleming, G. R. Excited-state proton transfer of protonated 1-aminopyrene complexes with .beta.-cyclodextrin. *J. Phys. Chem.* **1992**, *96*, 6904−6910.
(8) Chattopadhyay, N. Effect of cyclodextrin complexation on excited state proton transfer reactions. *J. Photochem. Photobiol., A* **1991**, *58*, 31−36.
(9) Maity, S. S.; Samanta, S.; Sardar, P. S.; Pal, A.; Dasgupta, S.; Ghosh, S. Fluorescence, anisotropy and docking studies of proteins through excited state intramolecular proton transfer probe molecules. *Chem. Phys.* **2008**, *354*, 162−173.
(10) Fleming, G. R. *Chemical Applications of Ultrafast Spectroscopy*; Oxford University Press: London, 1986.
(11) Birks, J. B. *Photophysics of Aromatic Molecules*; Wiley-Interscience: London, 1970.
(12) Valeur, B. *Molecular fluorescence: principles and applications*; Wiley-VCH: Weinheim, 2002.
(13) Zhu, H.; Fan, J.; Du, J.; Peng, X. Fluorescent Probes for Sensing and Imaging within Specific Cellular Organelles. *Acc. Chem. Res.* **2016**, *49*, 2115−2126.
(14) Kobayashi, H.; Ogawa, M.; Alford, R.; Choyke, P. L.; Urano, Y. New Strategies for Fluorescent Probe Design in Medical Diagnostic Imaging. *Chem. Rev.* **2010**, *110*, 2620−2640.
(15) Urano, Y.; Asanuma, D.; Hama, Y.; Koyama, Y.; Barrett, T.; Kamiya, M.; Nagano, T.; Watanabe, T.; Hasegawa, A.; Choyke, P. L.; Kobayashi, H. Selective molecular imaging of viable cancer cells with pH-activatable fluorescence probes. *Nat. Med.* **2008**, *15*, 104−109.
(16) Zhang, M.; Yu, M.; Li, F.; Zhu, M.; Li, M.; Gao, Y.; Li, L.; Liu, Z.; Zhang, J.; Zhang, D.; Yi, T.; Huang, C. A highly selective fluorescence turn-on sensor for cysteine/homocysteine and its application in bioimaging. *J. Am. Chem. Soc.* **2007**, *129*, 10322−10323.
(17) Garg, A.; Manidhar, D. M.; Gokara, M.; Malleda, C.; Reddy, C. S.; Subramanyam, R. Elucidation of the Binding Mechanism of Coumarin Derivatives with Human Serum Albumin. *PLoS One* **2013**, *8*, No. e63805.
(18) Wagner, B. The Use of Coumarins as Environmentally-Sensitive Fluorescent Probes of Heterogeneous Inclusion Systems. *Molecules* **2009**, *14*, 210−237.
(19) Stefani, H. A.; Gueogjan, K.; Manarin, F.; Farsky, S. H. P.; Zukerman-Schpector, J.; Caracelli, I.; Pizano Rodrigues, S. R.; Muscará, M. N.; Teixeira, S. A.; Santin, J. R.; Machado, I. D.; Bolonheis, S. M.; Curi, R.; Vinolo, M. A. Synthesis, biological evaluation and molecular docking studies of 3-(triazolyl)-coumarin derivatives: Effect on inducible nitric oxide synthase. *Eur. J. Med. Chem.* **2012**, *58*, 117−127.
(20) Zhang, W.; Li, Z.; Zhou, M.; Wu, F.; Hou, X.; Luo, H.; Liu, H.; Han, X.; Yan, G.; Ding, Z.; Li, R. Synthesis and biological evaluation of 4-(1,2,3-triazol-1-yl)coumarin derivatives as potential antitumor agents. *Bioorg. Med. Chem. Lett.* **2014**, *24*, 799−807.
(21) Yeggoni, D. P. R.; Manidhar, D. M.; Suresh Reddy, C.; Subramanyam, R. Investigation of binding mechanism of novel 8-substituted coumarin derivatives with human serum albumin and α-1-glycoprotein. *J. Biomol. Struct. Dyn.* **2016**, *34*, 2023−2036.
(22) Żamojć, K.; Wiczk, W.; Zaborowski, B.; Jacewicz, D.; Chmurzyński, L. Analysis of Fluorescence Quenching of Coumarin Derivatives by 4-Hydroxy-TEMPO in Aqueous Solution. *J. Fluoresc.* **2014**, *24*, 713−718.
(23) Dömötör, O.; Tuccinardi, T.; Karcz, D.; Walsh, M.; Creaven, B. S.; Enyedy, É. A. Interaction of anticancer reduced Schiff base coumarin derivatives with human serum albumin investigated by fluorescence quenching and molecular modeling. *Bioorg. Chem.* **2014**, *52*, 16−23.
(24) Chinnathambi, S.; Karthikeyan, S.; Rajendiran, M.; Udayakumar, K.; Manoharan, A.; Kandasamy, S.; Hanagata, N. 4-Hydroxycoumarin Derivative:N-(diphenylmethyl)-2-[(2-oxo-2H-chromen-4-yl)oxy]acetamide Interaction with Human Serum Albumin. *J. Spectrosc.* **2018**, *2018*, 1−14.
(25) Paul, S.; Roy, P.; Saha Sardar, P.; Majhi, A. Design, Synthesis, and Biophysical Studies of Novel 1,2,3-Triazole-Based Quinoline and Coumarin Compounds. *ACS Omega* **2019**, *4*, 7213−7230.
(26) Paul, S.; Ghanti, R.; Sardar, P. S.; Majhi, A. Synthesis of a novel coumarin derivative and its binding interaction with serum albumins. *Chem. Heterocycl. Compd.* **2019**, *55*, 607−611.
(27) Păunescu, E.; Louise, L.; Jean, L.; Romieu, A. A versatile access to new halogenated 7-azidocoumarins for photoaffinity labeling: Synthesis and photophysical properties. *Dyes Pigm.* **2011**, *91*, 427−434.
(28) Shigemitsu, H.; Matsuda, K.; Mori, T.; Nakatsuji, H.; Matsusaki, M.; Kida, T. Enhancing photostability of a coumarin dye by self-inclusion into a cyclodextrin cavity in aqueous solution and living cells. *Asian J. Org. Chem.* **2020**, *9*, 2112−2115.
(29) Szente, L.; Szejtli, J. Highly soluble cyclodextrin derivatives: Chemistry, properties, and trends in development. *Adv. Drug Delivery Rev.* **1999**, *36*, 17−28.
(30) Dsouza, R. N.; Pischel, U.; Nau, W. M. Fluorescent dyes and their supramolecular host/guest complexes with macrocycles in aqueous solution. *Chem. Rev.* **2011**, *111*, 7941−7980.
(31) Pal, A.; Sundar Maity, S.; Samanta, S.; Saha Sardar, P.; Ghosh, S. Interaction of the excited state intramolecular proton transfer probe 3-hydroxy-2-naphthoic acid with poly N-vinyl-2-pyrrolidone polymer in water: An insight into the water structure in the binding region. *J. Lumin.* **2010**, *130*, 1975−1982.
(32) Samanta, S.; Samanta, S. K.; Sanyal, S.; Mukherjee, M.; Sardar, P. S.; Ghosh, S. Features of partial encapsulation of an ESIPT probe 3-hydroxy-2-naphthoic acid (3HNA) in the nano cavities of β- and γ-cyclodextrin: comparative study with sequestered 3HNA in micelles and reverse micelle. *RSC Adv.* **2016**, *6*, 110610−110621.
(33) Turro, N. J. *Modern Molecular Photochemistry*; Benjamin/Cummings: Menlo Park, CA, 1978.
(34) Chakraborty, A.; Kar, S.; Guchhait, N. Photoinduced intramolecular charge transfer (ICT) reaction in trans-methyl p-(dimethylamino) cinnamate: A combined fluorescence measurement and quantum chemical calculations. *Chem. Phys.* **2006**, *320*, 75−83.
(35) Chipem, F. A. S.; Mishra, A.; Krishnamoorthy, G. The role of hydrogen bonding in excited state intramolecular charge transfer. *Phys. Chem. Chem. Phys.* **2012**, *14*, 8775−8790.
(36) Sarkar, N.; Das, K.; Datta, A.; Das, S.; Bhattacharyya, K. Solvation Dynamics of Coumarin 480 in Reverse Micelles. Slow Relaxation of Water Molecules. *J. Phys. Chem.* **1996**, *100*, 10523−10527.

https://doi.org/10.1021/acsomega.0c06152
ACS Omega 2021, 6, 11878−11896

(37) Liu, X.; Cole, J. M.; Low, K. S. Solvent Effects on the UV-vis Absorption and Emission of Optoelectronic Coumarins: a Comparison of Three Empirical Solvatochromic Models. *J. Phys. Chem. C* **2013**, *117*, 14731−14741.
(38) Abreu, A. S.; Hermenegildo, B. F. C.; Ferreira, P. M. T.; Queiroz, M. J. R. P.; Castanheira, E. M. S. Interaction of fluorescent quinolin-2-one and coumarin derivatives including dipeptides with lipid bilayers. *RSC Adv.* **2016**, *6*, 72141−72148.
(39) Bayraktutan, T.; Onganer, Y. Biophysical influence of coumarin 35 on bovine serum albumin: Spectroscopic study. *Spectrochim. Acta, Part A* **2017**, *171*, 90−96.
(40) Rang, H. P.; Dale, M. M.; Ritter, J. *Molecular Pharmacology*, 3rd ed.; Churchill Livingstone: New York, 1995.
(41) Dömötör, O.; Tuccinardi, T.; Karcz, D.; Walsh, M.; Creaven, B. S.; Enyedy, É. A. Interaction of anticancer reduced Schiff base coumarin derivatives with human serum albumin investigated by fluorescence quenching and molecular modeling. *Bioorg. Chem.* **2014**, *52*, 16−23.
(42) Rekharsky, M. V.; Inoue, Y. Complexation Thermodynamics of Cyclodextrins. *Chem. Rev.* **1998**, *98*, 1875−1918.
(43) Uekama, K.; Hirayama, F.; Irie, T. Cyclodextrin Drug Carrier Systems. *Chem. Rev.* **1998**, *98*, 2045−2076.
(44) Moyano, F.; Biasutti, M. A.; Silber, J. J.; Correa, N. M. New Insights on the Behavior of PRODAN in Homogeneous Media and in Large Unilamellar Vesicles. *J. Phys. Chem. B* **2006**, *110*, 11838−11846.
(45) Ganguly, A.; Ghosh, S.; Guchhait, N. Inclusion of an Anthracene-based Fluorophore within Molecular Containers: A Comparative Study of the Cucurbituril and Cyclodextrin Host Families. *J. Phys. Chem. B* **2016**, *120*, 4421−4430.
(46) (a) Chatterjee, A.; Maity, B.; Seth, D. Supramolecular Interaction between a Hydrophilic Coumarin Dye and Macrocyclic Hosts: Spectroscopic and Calorimetric Study. *J. Phys. Chem. B* **2014**, *118*, 9768−9781. (b) Hu, X.; Zhou, Z.; Han, L.; Li, S.; Zhou, W. Preparation and characterization of phloretin by complexation with cyclodextrins. *New J. Chem.* **2020**, *44*, 5218−5223.
(47) Kandoth, N.; Choudhury, S. D.; Mukherjee, T.; Pal, H. Host-guest interaction of 1,4-dihydroxy-9,10-anthraquinone (quinizarin) with cyclodextrins. *Photochem. Photobiol. Sci.* **2009**, *8*, 82−90.
(48) Li, S.; Purdy, W. C. Cyclodextrins and their applications in analytical chemistry. *Chem. Rev.* **1992**, *92*, 1457−1470.
(49) (a) Maity, B.; Chatterjee, A.; Ahmed, S. A.; Seth, D. Deciphering the perturbation effect of urea on the supramolecular host-guest interaction of biologically active hydrophobic molecule inside the nanocavity of cyclodextrins. *J. Lumin.* **2017**, *183*, 238−250. (b) Hunt, L. E.; Bourne, S. A.; Caira, M. R. Inclusion of Hydroxycinnamic acids in methylated cyclodextrins: Host-guest interactions and effects on guest thermal stability. *Biomolecules* **2021**, *11*, 45.
(50) Tabushi, I. Cyclodextrin catalysis as a model for enzyme action. *Acc. Chem. Res.* **1982**, *15*, 66−72.
(51) He, Y.; Fu, P.; Shen, X.; Gao, H. Cyclodextrin-based aggregates and characterization by microscopy. *Micron* **2008**, *39*, 495−516.
(52) Liu, J.; Yue, Y.; Wang, J.; Yan, X.; Liu, R.; Sun, Y.; Li, X. Study of interaction between human serum albumin and three phenanthridine derivatives: fluorescence spectroscopy and computational approach. *Spectrochim. Acta, Part A* **2015**, *145*, 473−481.
(53) Yue, Y.; Dong, Q.; Zhang, Y.; Li, X.; Yan, X.; Sun, Y.; Liu, J. Synthesis of imidazole derivatives and the spectral characterization of the binding properties towards human serum albumin. *Spectrochim. Acta, Part A* **2016**, *153*, 688−703.
(54) Majorek, K. A.; Porebski, P. J.; Dayal, A.; Zimmerman, M. D.; Jablonska, K.; Stewart, A. J.; Chruszcz, M.; Minor, W. Structural and immunologic characterization of bovine, horse, and rabbit serum albumins. *Mol. Immunol.* **2012**, *52*, 174−182.
(55) Sharma, K.; Yadav, P.; Sharma, B.; Pandey, M.; Awasthi, S. K. Interaction of coumarin triazole analogs to serum albumins: Spectroscopic analysis and molecular docking studies. *J. Mol. Recognit.* **2020**, *33*, No. e2834.
(56) Mukherjee, M.; Sardar, P. S.; Ghorai, S. K.; Samanta, S. K.; Roy, A. S.; Dasgupta, S.; Ghosh, S. A Comparative Study of Interaction of Tetracycline with Several Proteins Using Time Resolved Anisotropy, Phosphorescence, Docking and FRET. *PLoS One* **2013**, *8*, No. e60940.
(57) Nair, M. S. Spectroscopic study on the interaction of resveratrol and pterostilbene with human serum albumin. *J. Photochem. Photobiol., B* **2015**, *149*, 58−67.
(58) Yue, Y.; Liu, J.; Liu, R.; Dong, Q.; Fan, J. Binding of helicid to human serum albumin: A hybrid spectroscopic approach and conformational study. *Spectrochim. Acta, Part A* **2014**, *124*, 46−51.
(59) Ghosh, K.; Rathi, S.; Arora, D. Fluorescence spectral studies on interaction of fluorescent probes with Bovine Serum Albumin (BSA). *J. Lumin.* **2016**, *175*, 135−140.
(60) Abdelhameed, A. S.; Alanazi, A. M.; Bakheit, A. H.; Darwish, H. W.; Ghabbour, H. A.; Darwish, I. A. Fluorescence spectroscopic and molecular docking studies of the binding interaction between the new anaplastic lymphoma kinase inhibitor crizotinib and bovine serum albumin. *Spectrochim. Acta, Part A* **2017**, *171*, 174−182.
(61) Shi, J.-h.; Pan, D.-q.; Jiang, M.; Liu, T.-T.; Wang, Q. Binding interaction of ramipril with bovine serum albumin (BSA): Insights from multi-spectroscopy and molecular docking methods. *J. Photochem. Photobiol., B* **2016**, *164*, 103−111.
(62) Jiang, M.; Huang, C.-r.; Wang, Q.; Zhu, Y.-y.; Wang, J.; Chen, J.; Shi, J.-h. Combined spectroscopies and molecular docking approach to characterizing the binding interaction between lisinopril and bovine serum albumin. *Luminescence* **2016**, *31*, 468−477.
(63) Ratajczak, H.; Orville-Thomas, W. J. *Molecular Interaction*; Wiley, 1981.
(64) Reichardt, C. Solvatochromic Dyes as Solvent Polarity Indicators. *Chem. Rev.* **1994**, *94*, 2319−2358.
(65) Kamlet, M. J.; Abboud, J. L. M.; Abraham, M. H.; Taft, R. W. Linear solvation energy relationships. 23. A comprehensive collection of the solvatochromic parameters, .pi.*, .alpha., and .beta., and some methods for simplifying the generalized solvatochromic equation. *J. Org. Chem.* **1983**, *48*, 2877−2887.
(66) Datta, S.; Panja, S.; Mitra, P.; Halder, M. Distilbene Derivative as a New Environment-Sensitive Bifunctional Ligand for the Possible Induction of Serum Protein Aggregation: A Spectroscopic Investigation and Potential Consequences. *Langmuir* **2015**, *31*, 10781−10790.
(67) Benesi, H. A.; Hildebrand, J. H. A Spectrophotometric Investigation of the Interaction of Iodine with Aromatic Hydrocarbons. *J. Am. Chem. Soc.* **1949**, *71*, 2703−2707.
(68) Mallick, A.; Haldar, B.; Maiti, S.; Chattopadhyay, N. Constrained photophysics of 3-acetyl-4-oxo-6,7-dihydro-12H indolo-[2,3-a] quinolizine in micellar environments: a spectrofluorometric study. *J. Colloid Interface Sci.* **2004**, *278*, 215−223.
(69) Samanta, U.; Pal, D.; Chakrabarti, P. Environment of tryptophan side chains in proteins. *Proteins* **2000**, *38*, 288−300.
(70) Vivian, J. T.; Callis, P. R. Mechanisms of tryptophan fluorescence shifts in proteins. *Biophys. J.* **2001**, *80*, 2093−2109.
(71) Harvey, B. J.; Bell, E.; Brancaleon, L. A Tryptophan Rotamer Located in a Polar Environment Probes pH-Dependent Conformational Changes in Bovine β-Lactoglobulin A. *J. Phys. Chem. B* **2007**, *111*, 2610−2620.
(72) Chaturvedi, S. K.; Ahmad, E.; Khan, J. M.; Alam, P.; Ishtikhar, M.; Khan, R. H. Elucidating the interaction of limonene with bovine serum albumin: a multi-technique approach. *Mol. BioSyst.* **2015**, *11*, 307−316.
(73) Ahmad, E.; Rabbani, G.; Zaidi, N.; Ahmad, B.; Khan, R. H. Pollutant-Induced Modulation in Conformation and β-Lactamase Activity of Human Serum Albumin. *PLoS One* **2012**, *7*, No. e38372.
(74) Crosby, G. A.; Demas, J. N. Measurement of photoluminescence quantum yields. Review. *J. Phys. Chem.* **1971**, *75*, 991−1024.
(75) *FELIX 32, Operation Manual, Version 1.1*; Photon Technology International, Inc., 1009 Lenox Drive, Suite 104: Lawrenceville, NJ 08645, 2003.

https://doi.org/10.1021/acsomega.0c06152
ACS Omega 2021, 6, 11878−11896

(76) Hanwell, M. D.; Curtis, D. E.; Lonie, D. C.; Vandermeersch, T.; Zurek, E.; Hutchison, G. R. Avogadro: An Advanced Semantic Chemical Editor, Visualization, and Analysis Platform. *J. Cheminf.* **2012**, *4*, 17.
(77) Cameron, E. A.; Maynard, M. A.; Smith, C. J.; Smith, T. J.; Koropatkin, N. M.; Martens, E. C. Multidomain Carbohydrate-binding Proteins Involved in Bacteroides thetaiotaomicron Starch Metabolism*. *J. Biol. Chem.* **2012**, *287*, 34614−34625.
(78) Adachi, M.; Mikami, B.; Katsube, T.; Utsumi, S. Crystal Structure of Recombinant Soybean *β*-Amylase Complexed with *β*-Cyclodextrin. *J. Biol. Chem.* **1998**, *273*, 19859−19865.
(79) Feng, L.; Fawaz, R.; Hovde, S.; Sheng, F.; Nosrati, M.; Geiger, J. H. Crystal structures ofEscherichia colibranching enzyme in complex with cyclodextrins. *Acta Crystallogr., Sect. D: Struct. Biol.* **2016**, *72*, 641−647.
(80) Trott, O.; Olson, A. J. AutoDock Vina: improving the speed and accuracy of docking with a new scoring function, efficient optimization, and multithreading. *J. Comput. Chem.* **2010**, *31*, 455−461.
(81) Pettersen, E. F.; Goddard, T. D.; Huang, C. C.; Couch, G. S.; Greenblatt, D. M.; Meng, E. C.; Ferrin, T. E. UCSF Chimera?A visualization system for exploratory research and analysis. *J. Comput. Chem.* **2004**, *25*, 1605−1612.
(82) Berman, H. M.; Westbrook, J.; Feng, Z.; Gilliland, G.; Bhat, T. N.; Weissig, H.; Shindyalov, I. N.; Bourne, P. E. The Protein Data Bank. *Nucleic Acids Res.* **2000**, *28*, 235−242.
(83) Rarey, M.; Kramer, B.; Lengauer, T.; Klebe, G. A fast flexible docking method using an incremental construction algorithm. *J. Mol. Biol.* **1996**, *261*, 470−489.
(84) Hubbard, S. J.; Thorton, J. M. *'NACESS' Computer Program*; Department of Biochemistry and Molecular Biology, University College: London, 1993.

https://doi.org/10.1021/acsomega.0c06152
ACS Omega 2021, 6, 11878−11896